UCRL-8040 c. 2 repl.
Physics and
Mathematics

UNIVERSITY OF CALIFORNIA

Radiation Laboratory
Berkeley, California

Contract No. W-7405-eng-48

RECEIVED
LAWRENCE
BERKELEY LABORATORY

AUG 21 1987

LIBRARY AND
DOCUMENTS SECTION

DISINTEGRATION OF HELIUM BY 300-Mev NEUTRONS

William H. Innes

(Thesis)

November 1957

TWO-WEEK LOAN COPY

This is a Library Circulating Copy
which may be borrowed for two weeks.

Printed for the U. S. Atomic Energy Commission

UCRL-8040 c. 2 repl.

DISCLAIMER

This document was prepared as an account of work sponsored by the United States Government. While this document is believed to contain correct information, neither the United States Government nor any agency thereof, nor the Regents of the University of California, nor any of their employees, makes any warranty, express or implied, or assumes any legal responsibility for the accuracy, completeness, or usefulness of any information, apparatus, product, or process disclosed, or represents that its use would not infringe privately owned rights. Reference herein to any specific commercial product, process, or service by its trade name, trademark, manufacturer, or otherwise, does not necessarily constitute or imply its endorsement, recommendation, or favoring by the United States Government or any agency thereof, or the Regents of the University of California. The views and opinions of authors expressed herein do not necessarily state or reflect those of the United States Government or any agency thereof or the Regents of the University of California.

Contents

Abstract 4

I. Introduction 6

II. Experimental Procedure

1. Apparatus 8
2. Operation 9
3. Photography 9

III. Method of Analysis of Events 10

1. Available Data 10
2. Identification Procedure 11
3. Errors in Measurement 15
4. Calculations 17

IV. Corrections 21

1. Single-Pronged Stars 21
2. Two-Pronged Stars 22

V. Results and Discussion

1. Inelastic Events 24
2. Elastic Events 26
3. Meson Events 29
4. Cross Sections 29
5. Errors 31
6. Comparison with Theory 31
7. Comparison with Other Experiments 34
8. Energy and Angular Distributions 40

9. Oxygen Stars 43

10. Azimuthal Symmetry Check 45

VI. Conclusions 46

VII. Acknowledgments 48

Appendix

I. Definitions 49

II. Derivation of Formulas 50

Figures 54

References 73

DISINTEGRATION OF HELIUM BY 300-Mev NEUTRONS

William H. Innes

Radiation Laboratory
University of California
Berkeley, California

November 1957

ABSTRACT

An investigation of the inelastic and elastic reactions between high-energy neutrons and helium nuclei has been conducted with a cloud chamber filled with helium and operating in a pulsed magnetic field of 21,700 gauss. Neutrons produced by bombardment of a 1/2-inch LiD target with 340-Mev protons in the 184-inch synchrocyclotron were collimated and passed through the 22-inch expansion cloud chamber, which was filled with helium gas to a total pressure of 89.8 cm Hg. Exclusive of meson-producing reactions, the possible reactions are:

Inelastic	$He^4(n, pn)t$,
	$He^4(n, d)t$,
	$He^4(n, 2np)d$,
	$He^4(n, dn)d$,
	$He^4(n, 2n2p)n$,
	$He^4(n, 2n)He^3$;
Elastic	$He^4(n, n)He^4$.

The total number of events, for incident neutrons above 160 Mev, was normalized to the interpolated n-He^4 total cross section at 300 Mev, and absolute cross sections for the various processes were established. Energy and angular distributions of the reaction products have been

compared with available theoretical predictions and other experiments. A few cases of meson production were noted.

I. INTRODUCTION

There exists today a wealth of experimental data pertaining to the interactions of high-energy nucleons with other nucleons, simple nuclei, and complex nuclei. This information, much of which is concerned with neutron and proton interactions with nuclei ranging from the very lightest to the very heaviest, embraces incident nucleon energies ranging from a few Mev to the several-Bev energies of the Bevatron and the Cosmotron.

Despite this great amount and variety of data, or perhaps as a consequence, the outstanding problem of nuclear physics at the present time is the formulation of a satisfactory fundamental theory of nuclear forces--satisfactory in the sense that it not only unambiguously explains all the observed results but also can predict additional phenomena whose pursuit will lead to the orderly and rapid advance of nuclear science.

Increasing emphasis is being placed on experiments that may lead to an understanding of these forces. One of the most fruitful approaches in establishing models of the nucleus, and in revealing the behavior of several nucleons in close proximity, has been in scattering experiments with light nuclei, in which only a few nucleons are involved. As has been pointed out by Tannenwald,[1] the disintegration of helium presents an unique case because, while on the one hand there are so few particles involved that a theoretical analysis of the interactions between individual nucleons may be hoped for, it can also on the other hand show some of the properties of heavier nuclei, owing to the tightly bound structure of the helium nucleus. In particular, if the alpha particle indeed exists as a substructure in heavier nuclei, then helium disintegration will be of value in interpreting the structure and disintegration of heavier nuclei.

The identity, frequency of occurrence, and distributions in angle and energy of the secondary particles emitted in the disintegration of helium by high-energy neutrons are therefore expected to be useful in analyses of nuclear structure and of the nature of nuclear forces. For energies above a few Mev, however, there appears to be little

information in this area. Tracy and Powell, using a cloud chamber containing a mixture of helium and oxygen in a magnetic field of 13,000 gauss, studied secondary particles emitted under bombardment by 90-Mev neutrons;[2] analysis of helium data was complicated by the presence of large numbers of oxygen nuclei. Swartz, using a cloud chamber containing only helium and a small amount of water vapor, but without a magnetic field, studied secondary particles under bombardment by 200-Mev neutrons;[3] analysis of the data was complicated by the absence of a magnetic field. Tannenwald, using a cloud chamber containing only helium and a small amount of water vapor in a magnetic field of 22,000 gauss, studied helium disintegration by 90-Mev neutrons;[1] the absence of any significant number of other nuclei, and the use of a strong magnetic field, enabled him to make the first complete and detailed analysis of the identity and characteristics of secondary particles emitted in high-energy neutron bombardment of helium. Hillman, Stahl, and Ramsey have measured the total cross section of liquefied helium for 48-Mev and 88-Mev neutrons.[4] Moulthrop, using a high-pressure diffusion cloud chamber in a magnetic field of 21,000 gauss, studied negative pion production in the bombardment of helium by 300-Mev neutrons.[5] Theoretical predictions concerning the disintegration of helium by high-energy neutrons are also limited. Heidmann has analyzed the neutron-helium scattering problem, for incident neutron energies of 90 Mev and 200 Mev, using the Born approximation and Gaussian potentials and wave functions.[6,7]

The experiment presented herein extends the work of Tannenwald and Swartz to higher energies and, in a sense, supplements that of Moulthrop, who limited his complete analysis to those interactions which resulted in the production of pions. The cloud chamber is particularly adapted to studies of this type, as it presents the ultimate in "thin" targets, resulting in the best possible view of the associated particles in the reaction.

II. EXPERIMENTAL PROCEDURE

1. Apparatus

The neutrons produced by bombarding a 1/2-inch-thick LiD target with 340-Mev protons were collimated inside, through, and outside the concrete shielding of the 184-inch Berkeley synchrocyclotron by a 4-stage collimation system (see Figs. 13 and 14). The tapered lead collimator, inside the concrete shielding, was circular in cross section and 86.5 inches long, and had an exit diameter of 6 inches; the hole in the concrete shielding was circular in cross section, 208.0 inches long, with exit diameter of 12 inches; the first copper collimator, in the concrete shielding, was rectangular in cross section, 23/32 by 2-3/8 inches, and 34 inches long; the second (final) copper collimator, outside the concrete shielding, was rectangular in cross section, 1 by 3 inches, and 34 inches long. The neutrons entered the cloud chamber through a 1- by- 5-inch copper foil window, 3 mils thick, and passed out through a similar window to reduce backscattering from the exit wall of the chamber.

The Wilson cloud chamber used was developed by Powell[8] and has been used by him and others for a number of experiments. It is 22 inches in diameter, has a sensitive region 3-1/2 inches deep, and has a pressure-controlled expansion ratio. It fits into the 6-inch gap of a magnet capable of producing a pulsed field of 21,700 gauss.[8] The bottom of the chamber is a rubber-covered 1/2-inch-thick lucite disk which moves vertically and is controlled by a pantograph which keeps it accurately horizontal during the expansions. Gelatin containing a black dye covered the disk to a depth of 1/16 inch, providing a black background for track photography. General Electric FT 422 flash tubes were used on opposite sides of the chamber, providing uniform illumination over 2-1/2 inches of the 3-1/2-inch sensitive region.[9] The lamps were simultaneously flashed by the discharge, through each, of 512-microfarad condensers charged to a potential of 1700 volts.

2. Operation

The cloud chamber was operated in a pulsed magnetic field of 21,700 gauss which was energized by a current pulse of 4000 amperes supplied by a 150-hp generator with a 5-ton flywheel. The field requires about 2.5 seconds to attain its maximum value, where it remains steady for about 0.15 second before being turned off. The chamber was operated on a 1-minute automatically controlled cycle, as follows: the magnet current is turned on in advance so that its maximum coincides with the full expansion of the chamber; the cyclotron beam is pulsed through the chamber at the instant the moving diaphragm hits bottom, and the lights are flashed about 0.04 second after this. The current that passes through the magnet is recorded with each picture by an auxiliary lens which views a magnet-current meter. A clearing field of about 100 volts is removed just prior to expansion of the chamber and turned on again after the lights have flashed.

The chamber was filled with helium gas to a total pressure of 89.8 cm Hg in the expanded position; of this pressure, 1.7 cm was due to the partial vapor pressure of the water in the gelatin. The chamber was then compressed to a total pressure of about 103.0 cm, representing an expansion ratio of around 15%. The chamber and flash lights were surrounded by a felt-lined box and the whole kept at a constant temperature of 19.3°C by means of a temperature-controlled refrigerated water system.

3. Photography

A conical hole in the top pole piece of the magnet permits an automatic motor-driven camera to look down into the chamber and take paired stereoscopic photographs through twin 50-mm f/2 Leitz Summitar lenses spaced 4-1/2 inches apart. The camera is mounted 27 inches above the top glass of the chamber in a lighttight dome. Photographs are taken in sequence on 100-foot rolls of 1.8-inch-wide Eastman Linagraph Ortho film, which is developed to maximum contrast. Since the camera had no shutter, the length of exposure was determined by the length of the flash, about 100 microseconds.

All counting and measurement of events was made from the stereoscopic photographs. These were reprojected in the stereoscopic projector (diagrammed in Fig. 15). This projector has been developed for the general use of the Radiation Laboratory cloud chamber group, under Professor Wilson M. Powell; its construction and operation have been described elsewhere.[10] The projector duplicates the optical system of the camera-cloud chamber arrangement and, using the camera lenses, permits the reconstruction in space of events that occurred in the cloud chamber. This is accomplished by bringing the two track images into alignment on the translucent screen. The screen has three translational and two rotational degrees of freedom for this purpose.

III. METHOD OF ANALYSIS OF EVENTS

The use of a cloud chamber in studying nuclear reactions offers several advantages: a pure target can be used; the large solid angle of observation permits the detection of particles of all angles and energies; individual events can be studied in detail and, with the aid of a stereoscopic camera and projector, each charged-particle track can be reproduced in space in its original size, shape, and position; with the addition of a magnetic field, the momentum and energy of each charged particle can be determined. There are also limitations, chief of which is the relatively slow accumulation of data owing to the low target density.

1. Available Data

Following an outline by J. Tracy,[11] the data available for analyzing an event in this investigation may be divided into three categories. These are:

General Experimental Data. This includes knowledge of the direction and approximate energy distribution of the incident neutron beam, the direction and strength of the magnetic field, and the composition and stopping power of the gas mixture in the cloud chamber.

Individual Star Data. This includes information obtained from measurements on the individual tracks, such as initial radius of curvature, density, initial direction, range, rate of change of curvature, and rate of change of density.

Auxiliary Information. This includes application of the laws of conservation of momentum, total energy, and charge, as well as knowledge of range-energy relations, specific ionization vs energy relations, and characteristic track endings.

2. Identification Procedure

A comprehensive discussion of the ways in which the data outlined above may be used to identify charged particles in cloud chambers is available elsewhere.[1, 11, 12] There follows only a brief discussion of the particles here involved and of special situations whose existence sometimes enhanced the usual identification procedures.

Exclusive of meson-producing events, the possible reactions when a neutron strikes a helium nucleus are as follows. The brief symbol that appears on the right is used to represent the reaction to which it corresponds.

Inelastic Reactions		Symbol
$He^4(n, pn)t$	${}_0n^1 + {}_2He^4 \longrightarrow {}_1H^1 + {}_1H^3 + {}_0n^1$	[PT]
$He^4(n, d)t$	$\longrightarrow {}_1H^2 + {}_1H^3$	[DT]
$He^4(n, 2np)d$	$\longrightarrow {}_1H^1 + {}_1H^2 + 2\,{}_0n^1$	[PD]
$He^4(n, dn)d$	$\longrightarrow {}_1H^2 + {}_1H^2 + {}_0n^1$	[DD]
$He^4(n, 2n2p)n$	$\longrightarrow {}_1H^1 + {}_1H^1 + 3\,{}_0n^1$	[PP]
$He^4(n, 2n)He^3$	$\longrightarrow {}_2He^3 + 2\,{}_0n^1$	[He^3]
Elastic Reactions		
$He^4(n, n)He^4$	$\longrightarrow {}_2He^4 + {}_0n^1$	[He^4]

Analysis of an event involving the helium nucleus thus requires the identification of protons, deuterons, and tritons for two-pronged stars or the identification of He^3's and He^4's for one-pronged stars. Stars with three or more prongs are observed occasionally; they are due either to oxygen nuclei in the water vapor or to meson-production events with helium or oxygen. The relative number of oxygen nuclei can be computed from the partial pressures existing in the chamber, and in a subsequent section this is compared with the relative numbers of helium and oxygen stars observed. A few cases of meson production were noted; these also are discussed in a later section.

Two-Pronged Stars. The identification of the particles involved in the two-pronged stars rests mainly on measurements of their radii of curvature and an estimate of their relative ionizations. The fact that [DT] is a two-body problem requires that the two prongs be coplanar with the beam direction and that their transverse momenta be equal in magnitude and opposite in direction. These criteria can be used to fairly definitely establish an event as [DT] when verified by an alternate method of determining the energy of the incident neutron. They can be used, alone, more definitely to rule out [DT]: if one prong is definitely established as a deuteron (or as a triton) and the two prongs are not coplanar with the beam, then the other prong cannot be a triton (or a deuteron); similar reasoning applies if the transverse momenta do not sum to zero within reasonable limits.

It has been possible to identify the particles in the two-pronged stars in most cases. Out of 178 two-pronged stars that satisfied the ultimate selection criteria (dip angles within $\pm 50^{\circ}$ of the horizontal plane; incident-neutron energy equal to or greater than 160 Mev), 18 were not resolved with certainty during the film-reading process. Of these, 15 were recorded as either [PD] or [PT] and three as either [PD] or [DD]. These were resolved, after calculations for the incident-neutron energy for the alternative assumptions and study of the original data, as 11 [PD], 4 [PT], and 3 [DD]. If only these three types of events were considered, events (unweighted) were 66% [PT], 24% [PD], and 10% [DD] before resolution, and 62%,

28%, and 11% respectively, after the resolution.

One-Pronged Stars. Measurement of radius of curvature coupled with estimates of relative ionization was generally of little value in differentiating between He^3 and He^4. The tracks were most frequently of low energy, very dense, and often quite short. Their ionization, relative to minimum, falls in the range above 100, where estimates of relative density are insufficiently accurate; for the same radius of curvature the ionization of He^4 is only 50% greater than that of He^3. Tracks that ended in the chamber, with sufficient range, were identified by characteristic endings, and confirmed by comparison of observed and calculated ranges. When the track did not end in the chamber its change of radius with residual range was only rarely sufficient to effect a positive determination. Because of the large energy spread of the incident neutrons there are no unique energy-angle conditions that distinguish the particles with certainty. If the track goes backward in the chamber it cannot be an He^4 recoil associated with an incident neutron in the forward direction; this method of resolution also was rarely applicable. A track might be identified as He^3 on the basis that such choice results in a reasonable value for the energy of the incident neutron, whereas identification as He^4 would result in a neutron energy so large as to be completely unexplainable by errors in measurement.

Less than half the single tracks were identifiable with certainty during the film-reading process. Out of 66 one-pronged stars that satisfied the ultimate selection criteria (dip angles within $\pm 50^\circ$ of the horizontal plane; incident-neutron energy equal to or greater than 160 Mev) only 27 were identified. The results, based on the above outlined considerations, are summarized below:

	He^4	He^3
Characteristic endings	21	0
Radius change–residual range	3	1
Backward tracks	0	1
E_n excessive as He^4	0	1
	24	3

Less than one-third were identified by characteristic endings; in comparison, Tannenwald was able to so identify about one-half at 90 Mev.[1] No He^3 that on calculation satisfied the neutron-energy criterion were observed to end in the chamber; a few apparent ones, associated with neutrons of lower energy, had been so identified. At 90 Mev Tannenwald found only two, compared with 139 He^4.

Apportionment of the 39 unidentified tracks remaining, of the 66 here considered, in the ratios of the above table would yield 35 as He^4 and 4 as He^3. On the basis of a careful consideration of the resultant incident-neutron energies (minimum only in the case of He^3) when each of these 39 events was calculated as He^3 and as He^4, and of the similar results pertinent to the much greater number (454) of single-pronged events that resulted in a neutron energy of less than 160 Mev on either assumption, the final apportionment made was 36 to He^4 and 3 to He^3.

A table of ionization (relative to minimum) vs magnetic rigidity for protons, deuterons, tritons, He^3, and He^4, prepared by Donald Johnson,[13] was of great value. Alignment charts giving particle energy vs magnetic rigidity were essential during the film reading and subsequent calculations. (See Figs. 18-22.) The chart for protons is due to J. De Pangher;[14] others were constructed by the author.

Stopping Power. The stopping power of the gas mixture in the chamber immediately after expansion was calculated as 0.213 relative to dry air at 760 mm Hg and 15°C. Range-energy curves were prepared for each particle, from the data and techniques of Livingston and Bethe;[15] Aron, Hoffman, and Williams;[16] and Bethe.[17] The range-energy relations were checked experimentally for protons, tritons, and He^4. The energies of a few long tracks ending in the chamber were determined from their magnetic rigidity and their ranges measured with a long flexible ruler. The calculated and measured ranges agreed within 5 to 10%, which is within the experimental error expected. In addition, theoretical track endings were drawn and compared to the experimental track endings obtained; agreement was excellent.

3. Errors in Measurement

Complete analysis of an event requires, for the identification of the particles and subsequent calculations, measurements of radius of curvature, dip angle, beam angle, height of track in chamber at the point of curvature measurement, horizontal distance from point of curvature measurement to vertical axis of chamber, magnetic field strength, and total track length when track ends in the illuminated region of the chamber. The incident neutrons are assumed to enter the chamber in a parallel beam and the ratio of the number of stars observed in the collimated region to the number outside the region verifies this assumption.

Only those events which originated in a predetermined region of the chamber were analyzed. The acceptable region was determined primarily by the dimensions of the final collimator and was of rectangular cross section (1 inch high and 3 inches wide) with a length of 12 inches along the beam direction. This region was centered in the chamber so that its upper and lower defining planes were 2-1/4 and 1-1/4 inches from the chamber bottom.

Radius of Curvature. The curvature of a track is measured by reprojecting it life-size on a translucent screen oriented to contain the plane of the track, and then matching it with one of a series of arcs inscribed on a set of lucite templates. (See Fig. 15.) In the range of radii generally encountered the arcs increased in increments of 2% to 4% between successive curves. It was generally possible to conclude that only one curve was a best fit or, at worst, that the choice lay between two adjacent template arcs. In a number of past experiments experience has shown that the error in curvature measurement amounts to about 0.1 mm error in the sagitta independent of the particular curvature and track length; for a track of true radius 50 cm, with 20 cm of track available, this would result in a 1% error in radius-of-curvature determination. The uncertainties here are therefore assumed to be on the order of 3%. One picture in ten was taken without the magnetic field; from measurements of tracks made under these conditions it was concluded that errors due to turbulence

were negligible in comparison with the above measurement uncertainties.

Dip Angle and Beam Angle. Angular measurements rest on the verified assumption that all neutrons enter the chamber in a parallel beam; the chamber is aligned with the beam axis, vertically and horizontally. The accuracy of reprojection and of angular measurements with the apparatus used in this experiment has been extensively investigated by Powell et al.[10] They concluded that dip angles α could be determined to $\pm 1.5^{\circ}$ in the region 0° to 50°, and that beam angles β could be determined to $\pm 1^{\circ}$. (See Fig. 15 and Appendix I: Definitions.) The latter uncertainty includes the systematic error in aligning the reference cross marks on the top glass of the chamber with the direction of the neutron beam in the reprojection process.

Complete analysis of stars was limited to those events which had all their prongs within dip angles of $\pm 50^{\circ}$. This restriction was necessary because when the prong under consideration is too steep accurate superposition of the two stereoscopic images and accurate measurements of curvature and dip angle are impossible in a great many cases. Events with one or more prongs exceeding the 50° dip-angle restriction were recorded, and identified and analyzed to the extent possible. Geometrical correction factors, discussed in a subsequent section, were applied to each event that satisfied the dip-angle limitations, to take care of this imposed "blindness."

Magnetic Field. As previously noted, an ammeter in the camera dome indicating the magnet current is photographed simultaneously with the chamber pictures. A larger ammeter on the magnet-control panel also indicates this current, and its readings were recorded by an observer. The field strength is determined from these data and a magnetization curve. The magnet field varies by 6% over the region where tracks were measured, and an accurate map of the field is used to determine the field strength at the center of the measured part of the track. Since the field varies quite slowly over the useful region of the chamber, second-order corrections were not necessary.

The compounded errors of measurement of dip angle, curvature, and field strength enter into the calculated energy of the particle.

The probable error in energy determination is estimated as 5%.

4. Calculations

The analysis of an event is completed by making appropriate calculations for the particle energy, azimuthal angle ϕ, scatter or beam angle θ, and the energy (in some cases minimum only) of the incident neutron; for elastic scattering the scatter angle of the incident neutron in the center-of-mass system is also required. All calculations were made relativistically by use of formulas developed in Appendix II. As has already been indicated in Identification Procedure (III, 2), not all two-pronged events were unambiguously identified during the film-reading process, so that calculations under two assumptions as to particle identity were desirable; for one-pronged stars it was desirable to calculate each event both as $[He^4]$ and as $[He^3]$. A standard formula and uniform procedure for calculation, suitable to a CRC 102-A computer, were devised for computing the momentum and energy of the secondary neutron(s) and the incident neutron. This procedure was applicable to all types of events except [DT], which (as is shown below) is very easily calculated. Inputs were the energies and momentum components of the observed charged particles and the binding energies for the several reaction types. From the standpoint of simplicity of programming and over-all computer time it turned out that the simplest approach was to calculate each two-pronged event for every possibility except [DT], i.e., as [PT or TP], [PD or DP], [DD], and [PP], as well as computing each one-pronged event both as $[He^4]$ and as $[He^3]$. Sample calculation sheets, showing input data for the computer and computer outputs (indicated by arrows) are included in Appendix II. Calculations for the computer inputs were done with a desk calculator. Charged-particle scatter and azimuthal angles were similarly determined; charged-particle energies were determined with alignment charts. Center-of-mass-system scatter angle for the incident neutron in $[He^4]$ was by nomogram for the formula given in Appendix II.

Two-Pronged Stars. A total of 416 two-pronged stars was observed--293 that met the dip-angle limitations and 123 that did not. Of the 293 meeting dip-angle requirements only 178 turned out, on calculation, to have been induced by an incident neutron of energy equal to or greater than 160 Mev. Of the 123 not meeting dip-angle requirements calculations were possible for 94, and of these only 48 turned out to have been induced by an incident neutron of energy equal to or greater than 160 Mev; energy calculations in this group are not so reliable as those in the first. This breakdown is summarized in Table I.

Table I

Breakdown of calculations
for 416 two-pronged stars satisfying dip-angle requirements

Incident-neutron energy	Dip angle		
	Less than 50°	Greater than 50°	All
Greater than 160 Mev	178	48	226
Less than 160 Mev	115	46	161
Undetermined		29	29
	293	123	416

The [DT] process, being a two-body problem, is simply calculated. The deuteron and triton, both of which form visible tracks in the chamber, account for all the nucleons involved in the reaction. The energy of the incident neutron can be calculated as the sum of the charged-particle energies plus the binding energy of the reaction; it can also be independently calculated from the sum of the beam components of momentum of the deuteron and triton. The energies computed in these two ways should be equal within experimental error. Further checks are available: the transverse momenta of the deuteron and triton must be equal and opposite; the deuteron and triton must be separated by 180° in azimuthal angle. There was excellent conformance

with these requirements in the few [DT] cases observed.

In the [PT] and [DD] processes the two charged particles whose tracks are visible in the chamber account for only four of the five nucleons involved in the reaction; the path of the fifth particle, a neutron, is invisible. Since the direction of the incident neutron is known, only its energy and the beam and transverse-momentum components of the ejected neutron are undetermined. Available conservation-of-energy and -momentum relations are just sufficient to permit solution of the problem.

In the [PD] process two neutrons are ejected and there are too many unknowns to permit solution of the problem. By considering the two ejected neutrons as a single lumped particle of two neutron masses, and of momentum just sufficient to balance the event, an "incident-neutron energy" can be calculated. The energy so determined is only a minimum energy for the incident neutron, but it was calculated for the [PD] events.

The [PT] process, in which three neutrons are ejected, is also indeterminate. A minimum energy for the incident neutron was calculated by considering the three neutrons as a single lumped particle.

One-Pronged Stars. A total of 570 single tracks at least 2 cm long was observed--449 that met the dip-angle limitations and 121 that did not. For the 449 meeting dip-angle requirements, calculations were possible for 446 and of these only 66 turned out to have been induced by an incident neutron of energy at least 160 Mev. For the 121 not meeting dip-angle requirements calculations were possible for 108 and of these only 34 turned out to have been induced by an incident neutron of energy at least 160 Mev; energy calculations in this group are not so reliable as those in the first. This breakdown is summarized in Table II.

Table II

Breakdown of calculations
for 570 one-pronged stars satisfying dip-angle requirements

Incident neutron energy	Dip angle		
	Less than 50°	Greater than 50°	All
Greater than 160 Mev	66	34	100
Less than 160 Mev	380	74	454
Undetermined	3	13	16
	449	121	570

In addition, a total of 525 single tracks less than 2 cm long was observed. These tracks were simply recorded, and no measurements or calculations were attempted.

The $[He^4]$ elastic-scattering interaction can be simply calculated. A unique relativistically correct formula relates the incident-neutron energy to the observed energy and scattering angle of the recoil He^4 in the laboratory system. This formula is given in Appendix II and, although it is rather complex, is readily solved by a nomogram. Such a nomogram was constructed, but used only to check the solutions of the automatic computer, which used the uniform procedure already mentioned. The scatter angle θ' of the neutron in the center-of-mass system is given in terms of the recoil angle θ of the He^4 in the laboratory system by

$$\tan \theta = \sqrt{1 - \beta^2} \cot \frac{\theta'}{2},$$

where β is for the velocity of the center-of-mass system relative to the laboratory system. This formula was solved by a simple circular nomogram.

The $[He^3]$ process, in which two neutrons are ejected, is indeterminate. A minimum energy for the incident neutron was calculated by considering the two neutrons as a single lumped particle.

The formulas used in the above calculations, and the derivations of some, are given in Appendix II.

IV. CORRECTIONS

Because of the restriction of $\pm 50^{\circ}$ in dip angle in the film-reading process a geometrical correction factor must be applied to each measured event to determine the number of events that would have been observed without the restriction. For single tracks the correction factor is a function only of the beam angle θ of the observed particle; for two-pronged events the beam angles of both particles, and their difference in azimuth, are involved.

It has been assumed that all processes in this experiment occur with azimuthal symmetry and, as is shown in a subsequent section, the experimental data verify this assumption. For any given type of event, however, there is a range of azimuthal angles for which the corresponding dip angles exceed the arbitrarily imposed maximum dip angle. A corresponding number of events of this type, together with its associated properties (particle energies, scatter angles, etc.) are thus "lost". The geometrical correction factors are designed to recover these data.

1. Single-Pronged Stars

Consider an $[He^4]$ event in which the recoil helium nucleus has a scatter angle θ. From the isotropic distribution in azimuthal angle ϕ, we include in the measured data only those whose dip angle α given by

$$\alpha = \sin^{-1}(\sin\theta \sin\phi)$$

is equal to or less than some maximum, say α_0. Now, there is some value ϕ_0 of ϕ, less than 90°, for which one has

$$\sin^{-1}(\sin\theta \sin\phi_0) = \alpha_0 \quad .$$

Between ϕ_0 and 90° the dip angle would exceed α_0. In the first quadrant, therefore, only $\phi_0{}^\circ$ out of 90° yield measured data. The situation is repeated in the remaining three quadrants, so that we find this type of event in just $4\phi_0{}^\circ$ out of 360°. Thus, if N events of this type were observed in $4\phi_0{}^\circ$, we should have observed $N \times \frac{360}{4\phi_0}$ such events without the restriction in dip angle. The geometrical correction, or weighting factor, for this type of event is therefore $90/\phi_0$, where $\phi_0 = \sin^{-1}(\sin\alpha_0/\sin\theta)$. In Fig. 16 this correction factor has been plotted as a function of θ for $\alpha_0 = 50^\circ$; its maximum value, which occurs at $\theta = 90^\circ$, is seen to be 1.80.

2. Two-Pronged Stars

Consider a $\lfloor PT \rfloor$ event in which the proton has scatter angle θ_1, the triton has scatter angle θ_2, and the two tracks are separated in azimuth by an amount $\Delta\phi$. From the isotropic distribution we include in the measured data only those whose dip angles, given by

$$\alpha_1 = \sin^{-1}(\sin\theta_1 \sin\phi_1) \ ,$$

$$\alpha_2 = \sin^{-1}(\sin\theta_2 \sin\phi_2)$$

are simultaneously equal to or less than some maximum, say α_0. To determine the correction factor we need to find the azimuthal angular intervals that would satisfy the imposed condition for both the dip angles, with the added condition that ϕ_1 and ϕ_2 differ at all times by $\Delta\phi$. This was done graphically by means of Fig. 17, which is a plot of the relation

$$\phi = \sin^{-1}(\pm \sin 50^\circ / \sin\theta)$$

as θ varies from 50° to 130°.

The procedure was as follows: a transparent plastic triangle was laid over the figure; an ink dot was placed on the triangle at $\theta = \theta_1$ and $\phi = 0$ and a second dot placed at $\theta = \theta_2$ and $\phi = \Delta\phi$; the

triangle was then moved vertically through the plot, with the dots always on the ordinates at θ_1 and θ_2 respectively, so that the θ_1 dot moved from $\phi = 0^\circ$ to $\phi = 360^\circ$. So long as both dots are outside the ovals the conditions for including the event are satisfied. Consequently, if both dots are outside the ovals for $\Delta\phi_0{}^\circ$ during the sweep, the geometrical correction, or weighting factor, for this type event is simply $360/\Delta\phi_0$. It will be noted that the scale in θ is not complete; if either particle has a scatter angle equal to or less than 50° or equal to or greater than 130°, its corresponding dot would never enter an oval and the correction is more simply obtained from Fig. 16, based only on the second track; if the scatter angles of both the particles are in the intervals just defined, the weighting factor is unity. In practice most of the weighting factors were obtainable from Fig. 16, and ranged from unity to 1.8; a few required the use of Fig. 17, and were generally between 1.8 and 2.5, and one went as high as 3.2.

V. RESULTS AND DISCUSSION

1. Inelastic Events

Table III summarizes the results for those inelastic events which, having dip angles equal to or less than $\pm 50^{\circ}$, were subject to a detailed analysis and which also satisfied the condition that they were induced by an incident neutron whose energy was at least 160 Mev.

Table III

Summary of analysis for inelastic events of dip angle $\leqslant \pm 50^{\circ}$

Reaction	Actual number measured	Weighted number	Standard deviation (percent)
[PT]	103	150.1	9.9
[DT]	3	4.3	57.8
[PD]	46	67.5	14.7
[DD]	18	29.9	23.6
[PP]	8	12.3	35.4
[He^3]	6	9.5	40.8
Total	184	273.6	7.4

The weighted numbers are the total numbers of events of each type that would have been observed if the dip angle had not been restricted; they were determined by application, to each observed event, of the previously described geometrical correction factors. The deviations are statistical standard deviations based on the actual number of events measured as given in the second column.

As has been indicated in Table I, 48 two-pronged events were identified which met the requirement placed on incident-neutron energy but did not satisfy the dip-angle limitation; in addition there were 29 incompletely identified events (incident-neutron energy therefore indeterminate) which did not satisfy the dip-angle limitation. The former had a distribution among the several types of two-pronged events closely approximating that indicated in Table III; the latter can be arranged so as to give the same distribution. The distribution is indicated in Table IV.

Table IV

Distribution of identified two-pronged events

Dip-angle criterion	Reaction				
	/PT/ (%)	/DT/ (%)	/PD/ (%)	/DD/ (%)	/PP/ (%)
Acceptable (actual numbers)	57.9	1.7	25.8	10.1	4.5
Acceptable (weighted numbers)	56.8	1.6	25.6	11.3	4.7
Unacceptable (48 identified)	56.3	0.0	25.0	12.5	6.2

The 29 incompletely identified events were distributed as 18 /P?/, 5 /D?/ and 6 /T?/. Table I indicates that not less than half of them should be attributed to incident neutrons having energy of at least 160 Mev; their distribution is such that they could easily be arranged to conform to that in Table IV.

Discussion of Geometrical Correction. The difference between Columns 3 and 2 of Table III indicates that (exclusive of /He^3/ reactions) the geometric corrections have predicted the occurrence of 86 two-pronged events in the regions rejected by the dip-angle limitation. In comparison, 48 completely identified events satisfying the incident-neutron energy requirement and 29 incompletely identified events of unknown neutron

energy were actually observed. Reference to the third column of Table I reveals that 51%, or about 15, of the latter 29 events should be attributed to neutrons of at least 160 Mev; these, with the 48 identified events, total 63 where 86 were expected. However, it has been previously indicated that energy calculations for events that exceeded the dip-angle limitations were not particularly reliable; for the larger number of actual events that did not exceed the dip-angle requirement the second column of Table I indicates that 61% were due to neutrons of at least 160 Mev, and if this be applied to the 123 events that comprise the third column of Table I there result 75 where 86 are expected. It is concluded that, within the statistical errors of Table III, the 63 to 75 events actually observed in the excluded regions is compatible with the 86 predicted by the geometrical corrections.

The validity of the geometric correction applied to the single-pronged inelastic events, $[He^3]$, is discussed in the following section.

2. Elastic Events

Table V summarizes the results for those single-pronged events, primarily elastic, which, having dip angles equal to or less than $\pm 50^{\circ}$, were subject to a detailed analysis and which also satisfied the condition that they were induced by an incident neutron whose energy was at least 160 Mev.

Table V

Summary of analysis of single-pronged events (mostly elastic)

Reaction	Actual number measured	Weighted number	Standard deviation (percent)
$[He^4]$	60	104.3	12.9
$[He^3]$	6	9.5	40.8
	66	113.8	12.3

As before, the weighted numbers are the total numbers of each type that would have been observed if the dip angle had not been restricted. Standard deviations are based on the actual number of events measured as given in the second column.

As has been indicated in Table II, 34 single-pronged events were identified which met the incident-neutron energy requirement but did not satisfy the dip-angle limitation; in addition there were 13 unresolved events (incident-neutron energy therefore not determined) which did not satisfy the dip-angle limitation. The former were resolved as 32 $[He^4]$ and 2 $[He^3]$, which is not incompatible with the relative numbers of these events shown in the second column of Table V. Finally, 525 single tracks less than 2 cm long were observed.

Discussion of Missing Tracks. The angular distribution of the elastically scattered neutrons, in the center-of-mass system, shows a lack of neutrons in the forward direction; this is due to the short range of the recoils. (See Fig. 9.) Presumably these missing recoils are among the 525 tracks that were too short to measure. The experimental points of Fig. 9, which are relative values of $d\sigma/d\Omega$ as a function of the neutron scatter angle θ, have been fitted by the smooth gaussian drawn thereon. In Fig. 10 the 104.3 weighted $[He^4]$ events of Table V are plotted to show the number of neutrons scattered per 10° interval in the center-of-mass system. The experimental points of Fig. 10 are relative values of $(d\sigma/d\Omega)\sin\theta$; the curve is the corresponding function for the gaussian previously fitted to the data of Fig. 9. The experimental weighted events show 97.1 neutrons scattered at angles greater than 10°. When the area under the curve from 10° to about 57° is normalized to this number it is found that the area from 0° to 10° corresponds to 18.9 weighted events. Experimentally, only 7.2 weighted events were observed for the 0°- to - 10° interval. Thus approximately 11.2 weighted events are missing and should be among the previously mentioned very short tracks.

Examination of the second column of Table II shows that of the 449 single-pronged events whose associated neutron-energy determinations were the most reliable, 66 or about 15% were due to neutrons

of energy at least 160 Mev. If this ratio applied to the 525 very short tracks, then about 79 are available to account for the missing tracks. This is far more than is required; it is probable that a much smaller proportion of the very short tracks was actually induced by beam neutrons of at least 160 Mev.

In view of the above, the cross-section calculations in a subsequent section are based on the "corrected weighted total" of 97.1 + 18.9, or 116 elastic [He^4] events.

Discussion of Geometrical Correction. The difference between Columns 3 and 2 of Table V indicates that the geometric corrections have predicted the occurrence of 48 single-pronged events in the regions rejected by the dip-angle limitations. In comparison, 34 completely identified events satisfying the incident-neutron energy requirement, 13 unresolved events of unknown neutron energy, and 525 very short tracks of unknown angle and neutron energy were actually observed. If the 34 identified events be accepted as actually due to neutrons of energy greater than 160 Mev it can be shown that 4 of the 13 unresolved events and 16 of the 525 short tracks belong to the rejected regions and have the minimum required incident-neutron energy. These total 54, in good agreement with the 48 predicted by the geometrical corrections. However, while reasonably confident of the identification of the 34 events, the author is much less confident that they were all induced by neutrons of energy of at least 160 Mev. It has been previously indicated that energy calculations for events that exceeded the dip-angle limitation were not particularly reliable. If one compares the data in Columns 2 and 3 of Table II it is seen that the ratios therein of numbers of events due to neutrons of energy greater than 160 Mev to those due to neutrons of energy less than 160 Mev are widely divergent. The proportions of Column 2 are more reliable, and if they are applied to the 121 events which comprise Column 3 only 18 would be due to neutrons of the proper energy. Again it can be shown that 16 of the 525 short tracks (used above, and "correctly" derived in the first place) belong to the rejected regions

with the minimum required neutron energy. We thus arrive at 18 + 16, or only 34 where 48 were expected. It must therefore be concluded that something like 34 to 54 are found, with emphasis on the lower figure, where 48 are predicted, and that this is only marginal agreement within the statistical errors of Table V.

3. Meson Events

A careful search was made for meson-producing events. Three instances of negative-pion production in helium were observed, one by each of the reactions $He^4(n, pn\pi^-)He^3$, $He^4(n, d\pi^-)He^3$, and $He^4(n, dp\pi^-)d$. One possible case of positive-pion production was noted. These events have not been weighted because no restriction on dip angle was imposed. Since the thresholds for the reactions are approximately 200 Mev,[5] it is clear that they were induced by incident neutrons of energy greater than 160 Mev.

4. Cross Sections

In order to obtain absolute cross sections, the total number of weighted events, exclusive of pion events, comprised of 273.6 inelastic and 116 elastic events, has been normalized to an interpolated $n\text{-}He^4$ total cross section of 100 millibarns at 300 Mev. A standard deviation of 10% is estimated for this value. The interpolated total cross section was based on plots of σ_t vs $A^{2/3}$, the data used were those of Hillman et al.[4] for H, He, C, N, and O at 88 Mev; those of Taylor[18] for H, D, C, and O at 169 Mev; those of DeJuren,[19] Fox et al.,[20] and Nedzel[21] for H, D, Be, C, and O, at 270 Mev, 280 Mev, and 410 Mev respectively.

The results are listed in Table VI.

Table VI

Cross sections for inelastic and elastic events

Reaction	Cross section (mb)
Inelastic	
$He^4(n, pn)t$	38.5 ± 3.8
$He^4(n, d)t$	1.1 ± 0.6
$He^4(n, 2np)d$	17.3 ± 2.6
$He^4(n, dn)d$	7.7 ± 1.8
$He^4(n, 2n2p)n$	3.2 ± 1.1
$He^4(n, 2n)He^3$	2.4 ± 1.0
Elastic	
$He^4(n, n)He^4$	29.8 ± 3.8
$\frac{\sigma_{inel.}}{\sigma_t} = 0.70 \pm 0.10$	$\frac{\sigma_{el.}}{\sigma_t} = 0.30 \pm 0.06$

The cross section for negative-pion production is, from the few events observed, 0.8 ± 0.4 millibarn.

5. Errors

Measurement errors and the uncertainties encountered in the identification procedures have been discussed in Chapter III, Method of Analysis of Events. The probable error in energy determinations has been estimated as about 5%; this applies to observed particles for dip angles within the 50° limitation. Derived energies for incident neutrons are estimated to have an average probable error of about 10%, but those determinations involving large angles in elastic scattering were less reliable.

In the determination of cross sections and various angular and energy distributions the chief source of error is statistical. Only 244 acceptable events of all kinds were observed within the energy and angular limitations; although these were geometrically corrected to yield a weighted total of 390, the statistics are tied to the lower figure and its subdivisions and are not improved. Consequently, all other errors are considered negligible in comparison with the statistical errors.

In view of the above, the errors already quoted in Tables III, V, and VI, as well as those indicated in the several angular and energy distributions (Figs. 1-12), are statistical standard deviations based only on the number of events actually analyzed within the energy and angular limitations.

6. Comparison with Theory

The neutron-helium scattering problem, for monoenergetic neutrons of 90 Mev and 200 Mev, has been examined by Heidmann,[6,7] using the Born approximation and gaussian potentials and wave functions. Heidmann's theoretical relative cross sections are compared with the experimental findings of the study reported here in Table VII. No theoretical estimates are available for 300-Mev neutrons, and it should be noted that the neutron beam of this experiment exhibits a rather wide energy spectrum (Fig. 13) and further that the results are for neutrons of energy equal to or greater than 160 Mev. For a somewhat more realistic comparison, Heidmann's 90-Mev estimates are normalized to a total n-He^4 cross section of 200 millibarns,[4] and his 200-Mev estimates normalized

to a total cross section of 110 millibarns; the latter cross section is an interpolated estimate employing the data and procedure outlined in Section 4, Cross Sections (above).

Table VII

Comparison of various cross sections (in millibarns) from theory and experiment

Process		90 Mev, theory (Refs. 6, 22)	200 Mev, theory (Refs. 7, 23)	300 Mev, experiment
[PT]		49 ± 8	52 ± 12	38.5 ± 3.8
[DT]		13	6[a]	1.1 ± 0.6
[PD]		~2	~0	17.3 ± 2.6
[DD]		~0	~0	7.7 ± 1.8
[PP]		~0	~0	3.2 ± 1.1
[He^3]		~5	~5[b]	2.4 ± 1.0
[He^4]		131	47	29.8 ± 3.8
	Total	200	110	100

[a]Some liberties have been taken with Heidmann's estimates. His result for [DT] was 1/10 mb, with the statement that it was approximately two orders of magnitude too small.

[b]Heidmann made no estimate for [He^3] at 200 Mev. This value is obtained by taking 1/10 of his [PT] value, following his method of estimating this cross section at 90 Mev.

On consideration, first, of the gross features of this table it is seen that the theoretical predictions of Heidmann are in good agreement with the experimental observations of DeJuren and Moyer that total cross sections drop rapidly with energy above about 100 Mev and that this drop is primarily due to a decrease in the elastic part of the cross section.[24,25] The theoretical ratio of the elastic to the total cross section is about 0.65 at 90 Mev and about 0.43 at 200 Mev. Experimentally, Tannenwald observed a ratio of about 0.51 at 90 Mev[1] (actually neutrons of energy greater than 40 Mev in a spectrum peaked at about 75 Mev, and extending from about 40 to 115 Mev); Swartz observed a ratio of about 0.43 at 200 Mev[3] (actually neutrons of energy greater than 50 Mev in a spectrum peaked at about 195 Mev, and extending from about 50 to 230 Mev); this experiment yields a ratio of about 0.30 at 300 Mev (actually neutrons of energy greater than 160 Mev in a spectrum peaked at about 310 Mev, and extending from about 160 to 340 Mev).

The theory predicts $\lfloor PT \rfloor$ as the dominant process at both 90 Mev and 200 Mev, with relatively small variation of the cross section with energy; at 90 Mev the $\lfloor PT \rfloor$ cross section is about 37% of the elastic cross section designated $\lfloor He^4 \rfloor$, but at 200 Mev, because of the rapid drop in the elastic cross section, this ratio is about 1.1. This experiment shows that $\lfloor PT \rfloor$ continues to be the dominant process and varies perhaps a little more strongly with energy; the ratio of the $\lfloor PT \rfloor$ cross section to the elastic cross section is about 1.5, since the elastic cross section has decreased more rapidly than that of $\lfloor PT \rfloor$.

The theoretical cross section for $\lfloor DT \rfloor$ decreases substantially with energy from 90 Mev to 200 Mev. This is in agreement with the expected energy dependence of the direct pickup process;[26] theoretical considerations[27] and experiment[28] reveal a rapid decrease, with increasing energy, of the cross section for the formation of pickup deuterons by the direct pickup process. At 90 Mev Tannenwald observed that pickup deuterons made a substantial contribution to the $\lfloor DT \rfloor$ cross section, while at 200 Mev Swartz concluded that the $\lfloor DT \rfloor$ process seemed to have a very low probability. This experiment is in agreement with the theoretically predicted rapid decrease in the cross section for the $\lfloor DT \rfloor$

process; only three (unweighted) cases were observed within the energy and angular limitations.

Comparison of the theoretical predictions for [PD] and [DD] at 90 and 200 Mev with the experimental results at 300 Mev reveals that Heidmann's analytical procedure probably underestimates the frequency of these reactions. Tannenwald also found these processes to occur with significant frequency at 90 Mev.

For [PP] the theoretical predictions at the lower energies are in agreement with the results at 300 Mev; the complete disintegration of helium is relatively infrequent, even at the higher energies; Tannenwald obtained a similar result at 90 Mev.

The theoretical predictions for [He^3] at the lower energies are also in agreement with the 300-Mev results. As indicated in the footnote, Heidmann made no estimate for [He^3] at 200 Mev and the value in the table was obtained by using the procedure employed by him for the 90-Mev calculations. In those calculations Heidmann considered [PT] and [He^3] as similar processes of the first order and estimated the ratio of [He^3] to [PT] as

$$\left[1/4/(1/4 + 3/4)\right]\left(V_{Singlet}/V_{Triplet}\right)^2 ,$$

or about one-tenth. The experimental ratio at 300 Mev is about 1 to 16.

For the elastic-scattering case, [He^4], the theory predicts a significant decrease in cross section with increasing energy; the experimental results are in agreement.

Further comparisons of theory with experiment are found in Section 8, Energy and Angular Distributions (below).

7. Comparison with Other Experiments

Similar experiments have been conducted by Tannenwald at 90 Mev[1] and Swartz at 200 Mev;[3] Tannenwald's experiment was conducted with the same apparatus as described in this paper; the experiment by Swartz was also conducted with a cloud chamber, but analysis was difficult because no magnetic field was available.

Moulthrop, using a high-pressure diffusion cloud chamber in the magnetic field described herein, studied negative-pion production in the bombardment of helium by 300-Mev neutrons.[5] The results of Tannenwald and Swartz are compared with the present experimental findings in Table VIII; the results of Tannenwald and Moulthrop are compared with those of this experiment in Table IX, following the analogy originally employed by Moulthrop.[5] The experimental results at 90 Mev and 200 Mev have been normalized to total n-He^4 cross sections of 200 millibarns and 110 millibarns, respectively, as described in Section 6, Comparison with Theory (above).

Table VIII

Comparison of various cross sections (in millibarns) obtained at different energies

Process	90 Mev, experiment (Ref. 1)	200 Mev, experiment (Ref. 3)	300 Mev, experiment
[PT]	44.3 ± 6.3	62[a]	38.5 ± 3.8
[DT]	13.7 ± 2.6		1.1 ± 0.6
[PD]	15.8 ± 2.6		17.3 ± 2.6
[DD]	7.4 ± 1.6		7.7 ± 1.8
[PP]	0.8 ± 0.4		3.2 ± 1.1
[He^3]	16.9 (assumed)		2.4 ± 1.0
[He^4]	101.1 ±17.9	48	29.8 ± 3.8
Total	200	110	100
$\frac{\sigma_{inel.}}{\sigma_t}$	0.49 ± 0.07	0.43	0.70 ± 0.10

[a]Value for all inelastic processes; [DT] stated to be negligible

These experimental data illustrate, and are in good agreement with, the earlier observations that total cross sections drop rapidly with energy above about 100 Mev and that this drop is due primarily to the decrease in the elastic part of the cross section. The 90-Mev, 200-Mev, and 300-Mev total cross sections are 200, 110, and 100 millibarns, respectively, while the corresponding elastic cross sections are 101, 48, and 30 millibarns. The corresponding inelastic cross sections reveal significantly smaller energy dependence, particularly between 90 Mev and 200 Mev. In view of the relative uncertainties involved, Swartz's inelastic cross section is not incompatible with a steadily decreasing function of energy. As noted below, Tannenwald's inelastic cross section could be a little high, and his elastic cross section correspondingly low, because of his [He^3] assumption.

The 90-Mev and 300-Mev data agree that [PT] is the dominant inelastic process; the decrease of about 13% with energy is not great. There is also agreement that [PD] is next most frequent in occurrence; the increase of about 11% is not great. At 90 Mev, [DT] is third most frequent in occurrence, while at 300 Mev this process is negligible; the importance of the energy dependence of the direct pickup process in this reaction has already been discussed. The [DD] cross section appears to remain constant between 90 Mev and 300 Mev. The complete disintegration of helium, [PP], although still relatively insignificant, increases four fold from 90 Mev to 300 Mev.

There appears to be significant difference between the 90-Mev and 300-Mev values for [He^3]. It is possible that the 90-Mev value has been overestimated and that the 300-Mev value is underestimated. The same difficulties were encountered in both experiments in differentiating the helium isotopes He^3 and He^4 when their ranges did not end in the chamber. Tannenwald, at 90 Mev, estimated the [He^3] cross section as about one-third of [PT] plus one-third of that portion of the [DP] cross section attributable to pickup; Heidmann obtained a ratio of about one-tenth, as described above. Both estimates are based on the same phenomenological equivalence; [PT] and [He^3] can be considered as similar processes--in the former, the incident neutron interacts with

and strips a proton off the helium nucleus, while in the latter it interacts with and strips off a neutron. In this experiment special effort was made to identify $[He^3]$ events as described in Chapter III, Method of Analysis of Events. The experimental ratio of the $[He^3]$ cross section to the $[PT]$ cross section at 300 Mev is 1 to 16; Moulthrop observed a ratio of about 1 to 10 for the similar reactions in his experiment.[5] These results are in better agreement with Heidmann than with Tannenwald. In the 90-Mev experiment 23% of the tritons from $[PT]$ were observed to end in the chamber while only 5% of the He^3's (the total number of He^3's being based on the He^3 assumption) were observed to stop. At 300 Mev these percentages were 25% (based on actual number of events, or 23% based on weighted number of events) for tritons and zero for He^3's. As mentioned in Chapter III, no He^3 which on calculation satisfied the neutron-energy criterion were observed to end in the chamber; a few, associated with neutrons of lower energy, had been so identified; in point of actual numbers, Tannenwald found two definite He^3 endings. In view of the foregoing, although it is quite possible that (He^3) may have been underestimated in this experiment, it is believed that this process has been overestimated at 90 Mev. Of the three possible explanations advanced by Tannenwald for the observed great difference between phenomenologically similar processes, it appears that the most likely explanation is his first, viz., the number of He^3's was overestimated in the He^3 assumption.

As has already been mentioned, the behavior of the elastic cross section is as expected. In view of the above discussion, the elastic-cross-section value at 90 Mev may be somewhat higher, and that at 300 Mev somewhat lower, than indicated in Table VIII; the $[He^3]$ results affect the $[He^3]$ and $[He^4]$ cross sections and the ratio of the inelastic to the total cross section. It is perhaps worth noting that, with the assumption of an $A^{2/3}$ dependence, a straight-line extrapolation of Ball's measurements[29] of the inelastic cross section for 300-Mev neutrons on Pb, Cu, Al, and C targets gives $\sigma_{inel} = 70 \pm 10$ millibarns for helium.[5] From the straight-line fits by Millburn et al.[30]

to the experimental inelastic cross sections at 300 Mev (mainly the data of Ball) one can calculate the inelastic cross section for helium as 79 millibarns. Nedzel[21] has fitted the 270- to 280-Mev total cross sections to the transparent optical model of Fernbach, Serber, and Taylor;[31] if the constants so determined are applied to helium the calculated total cross section is 108 millibarns and the inelastic cross section is 82 millibarns. This experiment, which normalized the data to a total cross section of 100 millibarns, finds an inelastic cross section of 70.2 ± 5.2 millibarns.

Moulthrop, by invoking the principle of charge symmetry, has formulated a comparison among the inelastic cross sections for the several processes observed by Tannenwald (meson production not involved) and the relative cross sections observed in his own experiment for the corresponding processes involving negative-pion production;[5] the comparison was made for all processes except the pion-producing reaction $He^4(n, p\pi^-)He^4$, which is the analogue of the true elastic process $He^4(n, n)He^4$. The following table extends that originally prepared by Moulthrop, in comparing his own and Tannenwald's experiment, to include this experiment.

Table IX

Comparison of probabilities for reactions in which mesons are produced with those in which mesons are not produced

Meson-producing reactions		Non-meson-producing reactions		
Process	"Inelastic" at 300 Mev (%)	Process	Inelastic at 300 Mev (%)	Inelastic at 90 Mev (%)
$He^4(n, pn\pi^-)He^3$	34 ± 3	$He^4(n, pn)t$	55 ± 5	43 ± 5
$He^4(n, d\pi^-)He^3$	32 ± 3	$He^4(n, d)t$	2 ± 1	15 ± 3
$He^4(n, 2pn\pi^-)d$	16 ± 1	$He^4(n, 2np)d$	25 ± 4	16 ± 3
$He^4(n, dp\pi^-)d$	7 ± 1	$He^4(n, dn)d$	11 ± 3	8 ± 2
$He^4(n, 2p2n\pi^-)p$	2 ± 1	$He^4(n, 2n2p)n$	4 ± 2	1 ± 1
$He^4(n, 2p\pi^-)t$	4 ± 1	$He^4(n, 2n)He^3$	3 ± 1	17 (assumed)
$He^4(n, pn\pi^-)He^3$ or "elastic" i.e., $He^4(n, p\pi^-)He^4$	5 ± 1			
Totals	100		100	100
$\frac{\sigma_{inel.}}{\sigma_{total}}$	0.90 ± 0.03		0.70 ± 0.10	0.49 ± 0.07

In comparing his own and Tannenwald's experiments, the second and fourth columns above, Moulthrop called attention to the striking agreement in "inelastic" cross sections and noted that the "inelastic" cross sections, other than $He^4(n, pn\pi^-)He^3$ and $He^4(n, d\pi^-)He^3$, could be interpreted by the same sort of arguments as needed to understand the 90-Mev cross sections, and were not appreciably influenced by the production of a meson. Examination of the second and third columns of Table IX reveals that the analogy is not so striking at 300 Mev, but that it is certainly still qualitatively true.

Moulthrop also noted a real correlation between pion production and fast-deuteron formation ("fast" being applied to a particle of energy greater than 50 Mev). He observed the ratio "Fast Deuterons/(Fast Deuterons + Fast Protons)" to have the value of 0.38 ± 0.06 for negative-pion production in helium at 300 Mev, and cited the results of Ford[32] and Knapp[33] as 0.31 ± 0.06 and 0.5 (estimated) in similar pion-production experiments at 300 Mev for oxygen and deuterium respectively. The corresponding ratio for this experiment, without pion production, is 0.16, a value which tends to confirm the definite correlation noted by Moulthrop.

8. Energy and Angular Distributions

The $He^4(n, pn)t$ Reaction. Heidmann's predictions for this reaction at 90 Mev and 200 Mev are that the tritons are of low energy and emitted almost isotropically in the laboratory system.[6,7] At 90 Mev Tannenwald found that the angular distribution was not isotropic but concentrated in the forward direction; he found the triton energy distribution in excellent agreement with the prediction.[1] At 200 Mev Swartz observed that the distribution did not seem compatible with the predicted isotropic distribution.[3] The laboratory-system angular distribution of tritons in this experiment is shown in Fig. 1. It is very similar to that found by Swartz for all prongs; he was unable to deduce a distribution that could be definitely called that of tritons from [PT] alone. Figure 1 suggests a concentration in the forward direction, but not to the marked extent

observed by Tannenwald at 90 Mev. Figure 2 shows the energy distribution of the tritons in this experiment; agreement with prediction for the lower energies is excellent.

The proton angular distribution from [PT] events is shown in Fig. 3; it is very similar to that observed by Tannenwald at 90 Mev. Figure 4 shows the energy distribution of protons. In contrast to the observations of Tannenwald, at 90 Mev, that the number of protons per 20-Mev energy interval was maximum in the 0- to 20-Mev interval, and decreased steadily with energy, the distribution here is qualitatively suggestive of that which would be found for recoil protons in free n-p elastic scattering. This is illustrated by the superimposed curve, which is the nonrelativistic N(E) vs E for recoil protons from 340-Mev neutrons, normalized to the total number of events comprising the histogram.

The He^4(n, 2np)d Reaction. Figures 5 and 6 show the laboratory-system angular distribution and energy distribution, respectively, for the deuterons emitted in [PD] events; the deuterons tend to peak in the forward direction and to be of low energy. Figures 7 and 8 show the corresponding distributions for the protons of [PD] events. The protons tend to peak in the forward direction; in view of the poor statistics it is doubtful that the pronounced peak in the energy distribution for 120 to 160 Mev is real.

Other Inelastic Reactions. The [DT], [DD], [PP], and [He^3] reactions are of infrequent occurrence and there are not sufficient data for an attempt at determination of energy and angular distributions.

Elastically Scattered Neutrons. Heidmann has predicted the angular distribution in the center-of-mass system for neutrons elastically scattered by helium at 90 Mev and 200 Mev. The theoretical predictions are gaussian and centered on the forward direction, and are given by

$$\frac{d\sigma}{d\Omega} = 450\ e^{-7.86\,\theta^2} \text{ millibarns} \quad (90 \text{ Mev})$$
$$= 450\ e^{-17.5\theta^2} \text{ millibarns} \quad (200 \text{ Mev})$$

with angular half widths of about 17° and 11° respectively. These predictions show a rapid trend toward increasingly sharp peaking in the forward direction with increasing energy; with regard to the 200-Mev prediction, however, Heidmann states that, although the equation shows, that only about 1 in 10^7 are scattered to the rear, this particular result should be considered as valueless because of the neglect of the Fourier components corresponding to large changes of momentum and the use of Gaussian functions to permit analytic integrations.

Tannenwald found the 90-Mev experimental data not incompatible with a Gaussian distribution, and obtained a good fit by using an exponent of $-5\theta^2$. The angular half width corresponding to this equation is about 21°.

The angular distribution $d\sigma/d\Omega$ (in the center-of-mass system) of elastically scattered neutrons, from incident neutrons of energy equal to or greater than 160 Mev, found in this experiment is shown in Fig. 9. These data are also not incompatible with a Gaussian, and a good fit is obtained with the superimposed curve whose exponent is $-5.4\theta^2$; the angular half width is again about 21°, as found by Tannenwald at 90 Mev. These data are also shown in Fig. 10 as $d\sigma/d\theta = (d\sigma/d\Omega) \sin\ \theta$ and the corresponding curve for the empirical Gaussian fit has been superimposed. As described in Chapter V, Results and Discussion, the latter curve was used to correct the elastic data for tracks missed because they were too short to be measured.

It appears from the 90-Mev data of Tannenwald and the data of this experiment that the sharpness of the forward peak is substantially less than predicted by Heidmann and that the change between 90 Mev and 300 Mev is much less than would be expected from Heidmann's calculations.

Energy of Incident Neutrons. Figure 11 shows the energy distribution of the incident neutrons as derived from the elastic-scattering data; Fig. 12 shows this distribution as derived from the [PT], [DD] and [DT] data. Since [PD], [PP], and [He^3] permit calculation of a minimum neutron energy only, they have not been employed in these distributions. The energy spectrum of the incident-neutron beam given in Fig. 13 for a 1/2-inch LiD target is due to Ball,[29] and has been refined by De Pangher.[34] The smooth curve superimposed on Fig. 11 is obtained from the results of De Pangher normalized to the total number of events comprising the histogram. It is seen that the results of this experiment indicate a significantly greater number of neutrons in the 160- to 200-Mev interval than should be expected from the work of Ball and De Pangher. Although the similar curve has not been superimposed on Fig. 12 a greater number of 160- to 200-Mev neutrons is found here also. The statistics are poor in both cases.

9. Oxygen Stars

Because of the presence of water vapor in the cloud chamber a few oxygen stars were observed. Oxygen stars of two or more prongs originating in the acceptable region of the chamber, as described in Chapter III, Method of Analysis of Events, were recorded without the imposition of any restriction on dip angle. Their distribution, according to the number of prongs in the star, is given in the following table; the percentage distribution is also included together with that observed by Fuller in a study of the disintegration of oxygen by 300-Mev neutrons.[35]

Table X

Distribution of oxygen stars originating in cloud chamber under neutron bombardment

No. of prongs	Number observed	Distribution	
		This experiment (%)	Fuller (Ref. 35) (%)
2	21	52	42
3	10	25	29
4	5	13	12
5	3	7	12
6	1	3	4
7	0	0	1
	40		

The number observed can be compared with the number expected on the basis of the number of inelastic helium events observed, the inelastic cross sections of helium and oxygen, and the ratio of helium to oxygen nuclei in the cloud chamber. Since no dip-angle limitation was imposed on the oxygen stars, and no calculations were made of the energy of the incident neutrons involved, the number of inelastic helium events observed at all angles and energies and without weighting should be used; this number is 473. The inelastic cross section for helium is 70 millibarns from this experiment; interpolation in the data of Ball gives 255 millibarns for the inelastic cross section of oxygen.[29] The ratio of helium to oxygen nuclei in the chamber was 51.8. The calculated expected number of inelastic oxygen stars is 33 compared with the 40 that were actually observed.

10. Azimuthal Symmetry Check

It has been assumed that all processes in this experiment occurred with azimuthal symmetry, and this assumption has been the basis for the geometric correction factor applied in weighting the observed events. It is desirable to verify this assumption by an examination of some of the azimuthal distributions involved. The following table shows the number of $[He^4]$ recoils, and tritons from $[PT]$, actually observed in four azimuthal angular intervals.

Table XI

Azimuthal distribution of $[He^4]$ recoils and tritons from $[PT]$

	Azimuthal angular interval			
	0° - 50°	130° - 180°	180° - 230°	310° - 360°
He^4 recoils	19 ± 6	30 ± 7	31 ± 7	23 ± 6
Tritons from $[PT]$	32 ± 7	37 ± 8	32 ± 7	24 ± 6

The uncertainties are standard deviations based on the number of events actually observed.

VI. CONCLUSIONS

In the bombardment of helium by 300-Mev neutrons the dominant reaction is inelastic scattering, which accounts for 70% of the total cross section. Of the six possible inelastic reactions (exclusive of meson-producting reactions) the most frequent is [PT], in which the incident neutron strips a proton from the helium nucleus, leaving a low-energy triton; [PT] accounts for 55% of the inelastic cross section. The phenomenological analogue of this process, [He^3], in which the incident neutron strips a neutron from the helium nucleus and leaves a low-energy He^3 nucleus, is negligible at this energy and accounts for about 3% of the inelastic cross section. The [DT] process is also negligible at this energy, accounting for about 2% of the inelastic cross section. The [PD] process contributes 25%, and the [DD] process 11%, of the inelastic cross section. The complete disintegration of helium, [PP], is rare and contributes about 4% of the inelastic cross section. With the exception of [DT] and (He^3) these results are similar to those found in a similar experiment at 90 Mev.[1] At the lower energy about half the [DT] cross section was contributed as a special case of [PT] through the pickup process in which the proton and outgoing neutron form a high-energy forward deuteron; the pickup portion of [DT] would be expected to be neglible at 300 Mev. A direct comparison with theory is not possible, but qualitative comparisons may be made with predictions made for 90 Mev and 200 Mev.[6,7] Such comparisons reveal agreement in the cross section for [PT], but not in the angular distribution of the associated tritons, and indicates that the theory probably greatly underestimates the frequency of [PD] and [DD]; similar conclusions obtained for the 90-Mev experiment.

Elastic scattering exhibits the expected forward peak of scattered neutrons in the center-of-mass system. The differential cross section for elastic scattering is not incompatible with a gaussian distribution, of angular half width about 21°, and is quite similar to that found in the 90-Mev experiment. The sharpness of the forward peak is considerably less than would be expected from qualitative extrapolation of the available theoretical predictions.

A small cross section for negative-pion production in helium, and some evidence supporting a possible correlation between pion production and fast deuteron formation,[5] have been observed.

VII. ACKNOWLEDGMENTS

The author wishes to acknowledge his indebtedness to Professor Wilson M. Powell for suggesting the experiment and for making available the extensive facilities of the University of California Radiation Laboratory cloud chamber group; and particularly for his counsel, continuing interest, and active participation throughout the investigation.

Many members and former members of the cloud chamber group contributed in one way or another to the completion of this experiment, and their cooperation is acknowledged with pleasure. Special thanks are due to Dr. Franklin C. Ford, Dr. Chung Ying Chih, and Messrs. John B. Elliott, Larry O. Oswald, and Milton M. Hill, who furnished valuable technical assistance. Mrs. Dorothy J. Gardner developed the stereoscopic negatives.

Special thanks are also due to Mr. S. C. Hight, Direction of Research, Sandia Corporation, for making available the computer facilities of the Sandia Corporation, and to Miss M. K. Weston and Mrs. E. G. Young, who programmed the computations and ran them on the CRC 102-A computer.

This work was performed under the auspices of the Atomic Energy Commission.

APPENDIX

I. DEFINITIONS

Dip angle α	The angle between the initial direction of the track and its projection on the horizontal plane containing the neutron beam.
Beam angle β	The angle between the projection of the initial track direction on the horizontal plane and the direction of the neutron beam.
Scatter angle θ	The angle between the initial track direction and the neutron beam.
Azimuthal angle ϕ	The angle between the projection of the initial track direction on a plane perpendicular to the neutron beam, and the horizontal plane.
Slant radius ρ_s	The radius of curvature of the track as measured in the slant plane.
Radius ρ	$\rho = \rho_s \cos \alpha$ is the radius of curvature that a particle of slant radius ρ_s would have if it were moving with the same momentum in a plane perpendicular to the magnetic field.
Slant plane	The plane containing the initial track direction and the horizontal line perpendicular to the initial track direction. It is approximately the plane of the track except that, in general, the path of a charged particle in a magnetic field describes a helix. The slant plane is at dip angle α to the horizontal plane.
Transverse momentum	$H\rho_t = H\rho \sin \theta$
Momentum in the beam direction	$H\rho_z = H\rho \cos \theta$

II. DERIVATION OF FORMULAS

1. General Formula for All Reactions Except [DT]

Consider the collision of a fast particle (neutron) of kinetic energy T_n, total energy E_n, and rest mass m, with a second particle at rest (helium nucleus) of total energy E_M and rest mass M. After the collision we observe charged particles Nos. 1 and 2 of kinetic energy T_1 and T_2, total energy E_1 and E_2, and rest mass m_1 and m_2. Present, but not visible, is the path of an uncharged particle of kinetic energy $T_{n'}$, total energy $E_{n'}$ and rest mass m'.

Introduce a set of rectangular coordinates with the positive direction of the z axis coinciding with the momentum vector of the incident particle; let subscript z denote z components of momentum and subscript t denote transverse components of momentum. Conservation of total energy and momentum requires

$$E_n + E_M = E_1 + E_2 + E_{n'},$$
$$P_n = p_{1z} + p_{2z} + p_{n'z},$$
$$0 = p_{1t} + p_{2t} + p_{n't},$$

where $p^2 = p_z^2 + p_t^2$ for each particle.

These equations are just sufficient to determine the three unknowns of the problem, namely, $p_{n'z}$ and $p_{n't}$ (whence $p_{n'}$ and $E_{n'}$) and p_n (whence E_n). Denoting $E_1 + E_2 - E_M$ by Σ in the first of the above equations; and $p_{1z} + p_{2z}$ by P in the second; and introducing the relativistic relation between total energy and momentum, we can write

$$E_n = \Sigma + E_{n'}, \tag{1}$$
$$E_n^2 = c^2 p_n^2 + (mc^2)^2, \tag{2}$$
$$E_{n'}^2 = c^2 p_{n'}^2 + (m'c^2)^2. \tag{3}$$

Squaring Eq. (1) and substituting the resulting expression for E_n^2 into Eq. (2) gives

$$\Sigma^2 + 2E_{n'}\ \Sigma + E_{n'}^2 = c^2(P + p_{n'z})^2 + (mc^2)^2 \quad . \qquad (4)$$

Substituting $E_{n'}$ and $E_{n'}^2$ from Eq. (3) into (4) gives, after considerable simplification, a solution of the quadratic equation in $p_{n'z}$ as follows:

$$p_{n'z} = \frac{e}{c}\ \frac{(zH\rho)_z \left\{9(zH\rho)_z^2 - 9(zH\rho)_t^2 + 10^8\left[(mc^2)^2 - (m'c^2)^2 - \Sigma^2\right]\right\}}{2\left[10^8\ \Sigma^2 - 9(zH\rho)_z^2\right]}$$

$$\pm\ \frac{e}{c}\ \frac{10^4}{3}\ \Sigma\ \frac{\left[\left\{9(zH\rho)_z^2 - 9(zH\rho)_t^2 + 10^8\left[(mc^2)^2 - (m'c^2)^2 - \Sigma^2\right]\right\} - 4\left\{10^8\Sigma^2 - 9(zH\rho)_z^2\right\}\left\{9(zH\rho)_t^2 + 10^8(m'c^2)^2\right\}\right]^{1/2}}{2\left[10^8\ \Sigma^2 - 9(zH\rho)_z^2\right]},$$

where all energies are in Mev, $p_{n'z}$ is in Mev/c, the notation $(zH\rho)_z$ is equivalent to $(z_1H_1\rho_1)_z + (z_2H_2\rho_2)_z$, and similarly for $(zH\rho)_t$ where z_1 and z_2 are the particle charge numbers.

This result can be written in the symbolic form,

$$\frac{c}{e}\ p_{n'z} = \frac{A(H\rho)_z\ [\ ] \pm \frac{10^4}{3}\ \Sigma\ [\ ]^2 - 4\ \Delta\ \sigma}{2\ \Delta},$$

where A is either 1 or 2 and $[\ ]$, Δ, and σ are all functions of Σ, $(H\rho)_z$, and $(H\rho)_t$. A program involving only these three quantities as inputs can be prepared for solution by an automatic computer.

Considerable numerical simplification is possible if it is kept in mind that: for /PT/ and /DD/ only one neutron is ejected so that one has $m' = m$; for /PD/ two neutrons are ejected, but can be lumped for a minimum-energy solution, so that one has $m' = 2m$; for /PP/ three

neutrons are ejected, but can be lumped for a minimum solution, so that one has $m' = 3m$; for $[He^3]$ only one charged particle is involved, so that one has $m_2 = 0$, and two neutrons are ejected so that one has $m' = 2m$ for a minimum solution; for $[He^4]$ only one charged particle is involved, so that one has $m_2 = 0$, and only one neutron is ejected so that one has $m' = m$; and finally, for all cases,

$$\Sigma = E_1 + E_2 - E_M = T_1 + T_2 + m_1c^2 + m_2c^2 - Mc^2 .$$

The computer obtains $\frac{c}{e}\, p_{n'z}$ in units of gauss-cm x 10^{-5}, solves for $T_{n'}$ and T_n in Mev, and prints out the results. Sample calculation sheets, showing the data read from the cloud chamber photographs, the derived computer inputs, and the computer results appear at the end of this Appendix.

2. Formulas for the [DT] Reaction

This is the two-body problem and T_n can be calculated in two ways:

$$T_n = T_1 + T_2 + BE,$$

$$T_n = m_0c^2\left[\sqrt{1 + \frac{c^2p^2}{(m_0c^2)^2}} - 1\right].$$

The second solution is obtained with sufficient accuracy by use of the alignment chart for protons (Fig. 18), taking p in gauss-cm as the sum of the observed $(H\rho)_z$ values of the deuteron and triton.

3. Formulas for $[He^4]$ Neutron-Scattering Angle

It can be easily shown that the scattering angle of the elastically scattered neutron in the center-of-mass system is related to the recoil angle of the helium nucleus in the laboratory system by

$$\tan\theta = \sqrt{1 - \beta^2}\,\cot\frac{\theta'}{2}\,, \qquad \text{(A1)}$$

where θ is the recoil angle of the helium nucleus in the laboratory system, θ' is the corresponding scatter angle of the neutron in the center-of-mass system, and $\beta = v/c$ for the velocity of the center-of-mass system relative to the laboratory system. For n-He^4 elastic scattering one has

$$1 - \beta^2 = \frac{8\left(\frac{T_n}{m_0c^2} + 1\right) + 17}{\left(\frac{T_n}{m_0c^2} + 5\right)^2} . \qquad \text{(A2)}$$

Equation (A1) is easily solved by a simple circular nomogram with a family of indices, determined from Eq. (A2), for T_n = 200, 250, 300, and 350 Mev.

4. Binding Energies

Process	Binding Energy (Mev)
[PT]	19.8
[DT]	17.6
[PD]	26.0
[DD]	23.8
[PP]	28.1
[He^3]	20.5

PT

Range Factor: 1.205 Picture: 646 I

Magnet Current: 4005

Origin: h = 1.4, r = 1.4

Track	R°	R_T	Comment		α	β	θ	φ	H ($\times 10^{-4}$)	P_s°	Observed $H\rho$	Corrected $H\rho$ ($\times 10^{-5}$)
											P	99.0
											d	51.4
				Cos	.976	.914	.892		h° 0.9		t	26.6
				Sin	.216	.407	.454	.476	r° 2.6	z° 5.9		
1	—	—	14.8 cm. width		-12.5	-24.0	27.0	28.5	2.220	68	14.73	14.73
											P	11.1
											d	5.6
				Cos	.998	.959	.954		h° 1.3		t 2.80	2.7
				Sin	.165	.284	.301	.669	r° 1.3	z° 7.2		
2	—	—	21° cm. width		+6.0	-162.5	162.5	339.5	2.175	21	4.55	4.71

$\Delta\varphi = 311$

$\cos\theta = \cos\alpha \cos\beta$

$\sin\varphi = \sin\alpha / \sin\theta$

	$(H\rho)_z$	$(H\rho)_h$	Σ (P,t)	(t,P)	(d,d)	(P,d)	(d,P)	(P,P)
1	+13.14	-6.69	T_1 99.0	24.6	51.4	99.0	51.4	99.0
2	-4.61	-1.45	T_2 3.7	11.1	5.6	5.6	11.1	11.1
			19.81	19.81	23.02			
						-913.50	-913.50	-1850.79
	+	—						
	7.53	7.14	122.5	65.5	76.7	208.9	551.0	1740.6
		ΣR_h	18.41	8.46	10.81	11.65	7.66	11.02
		T_n	299.5	129.2	164.5	177.1	118.0	167.9
		T_1'	173.1	66.7	93.5	42.7	29.7	29.5
		T_1	99.0	24.6	51.4	99.0	51.4	99.0
		T_2	3.7	11.1	5.6	5.6	11.1	11.1
		B.G.	19.81	19.81	23.02	25.98	25.98	28.14
		Clear T_n	299.6	129.3	164.6	177.3	118.2	167.0

$(H\rho)_z$ $\lvert\theta\rvert$	$(H\rho)_z$	$(H\rho)_t$ α	$(H\rho)_t$
<90	+	+	+
>90	−	−	−

Sign of α, β

$\lvert\theta\rvert$	θ
<90	$\lvert\theta\rvert$
>90	$180-\lvert\theta\rvert$

α	β	φ
−	−	$\lvert\varphi\rvert$
−	+	$180-\lvert\varphi\rvert$
+	+	$180+\lvert\varphi\rvert$
+	−	$360-\lvert\varphi\rvert$

Sign of φ

Weight Factor: 1.00

MU-14473

He^4

Range Factor: 1.210 Picture: 712M

Magnet Current: 4000

Origin: h= r=

Track	R^*	R_T	Comment		α	β	θ	ϕ	H	P_s^*	Observed Hp	Corrected Hp
				Cos	.982	.151	148		h° —			
		15.44		Sin	.191	.988	989	.193	r° —	.0 —	He^4 16.1	4.1
He^4	—	12.5	Ends He^4		+11	-81	81.5	3480				2.91
											He^3 3.7	5.5
He^3												2.91

$\cos\theta = \cos\alpha \cos\beta$

$\sin\phi = \sin\alpha / \sin\theta$

Relastic Neutron Scatter c.o. 16.9

	$(Hp)_z$	$(Hp)_z$	Σ	
	Cos θ	Sin θ	He^4	He^3
			0	-918.96
Input Data He^4	+0.431	-2.38	4.1	
He^3				918.4

$(Hp)_z$	
|β|	|Hp|
<90	+
>90	−

$(Hp)_z$	
β	|Hp|
+	+
−	−

θ

|β|	θ
<90	|θ|
>90	180−|β|

φ

α	β	φ
−	−	|φ|
−	+	180−|φ|
+	+	180+|φ|
+	−	360−|φ|

Output Data

$\frac{1}{2}P_{s_1}$	25.28	10.52
T_0	283.9	60.1
T_n'	279.8	34.1
T_1	4.1	5.5
B.E.	0	20.53
Check T_0	283.9	60.1

Weight Factor: 1.76

MU-14472

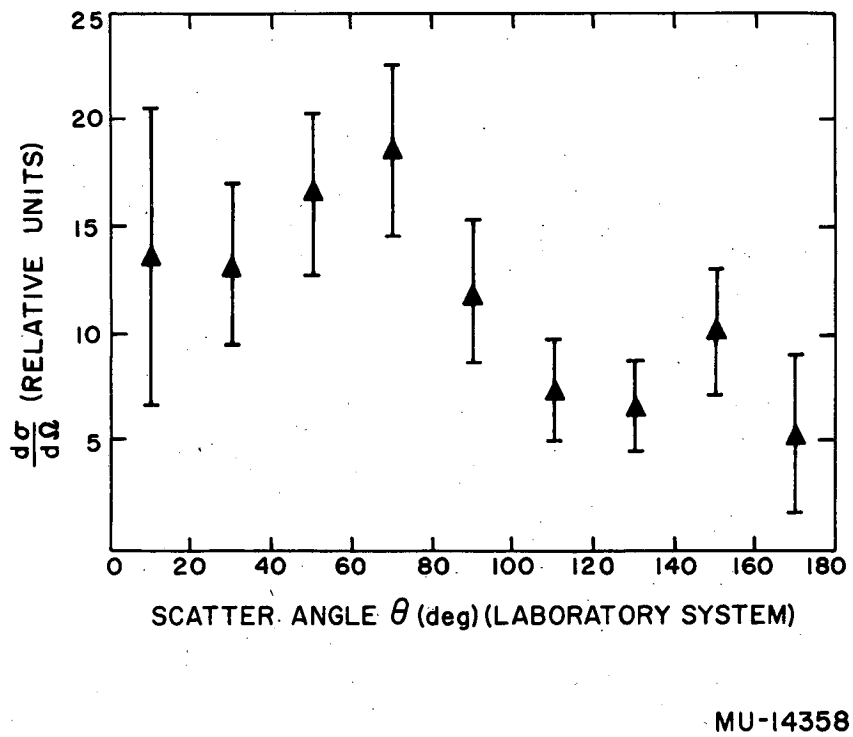

Fig. 1. Angular distribution of tritons from $\lfloor PT \rceil$ events.

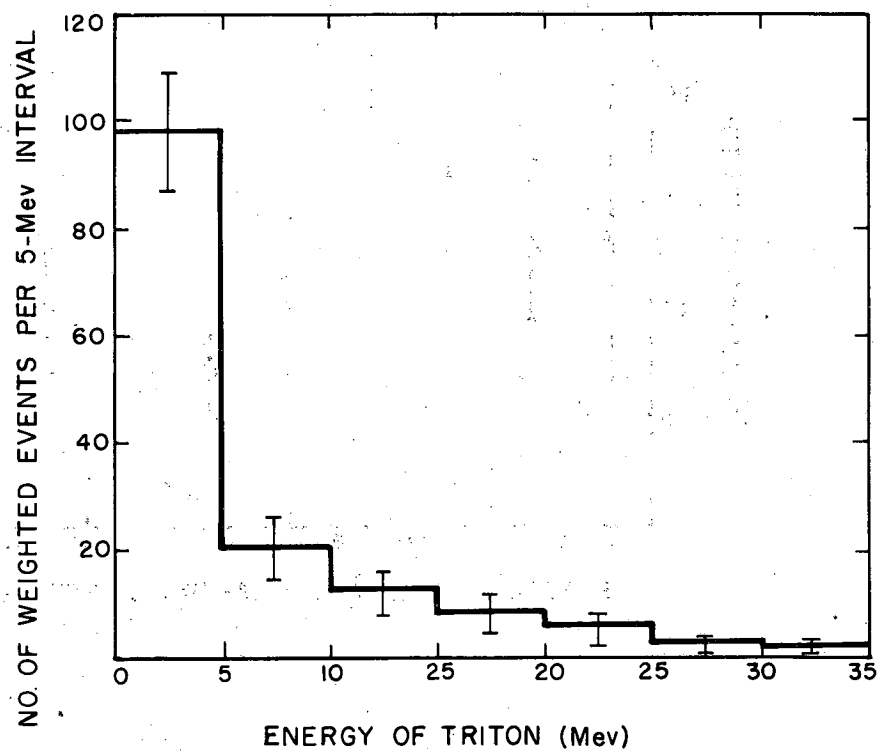

MU-14359

Fig. 2. Energy distribution of tritons from [PT] events.

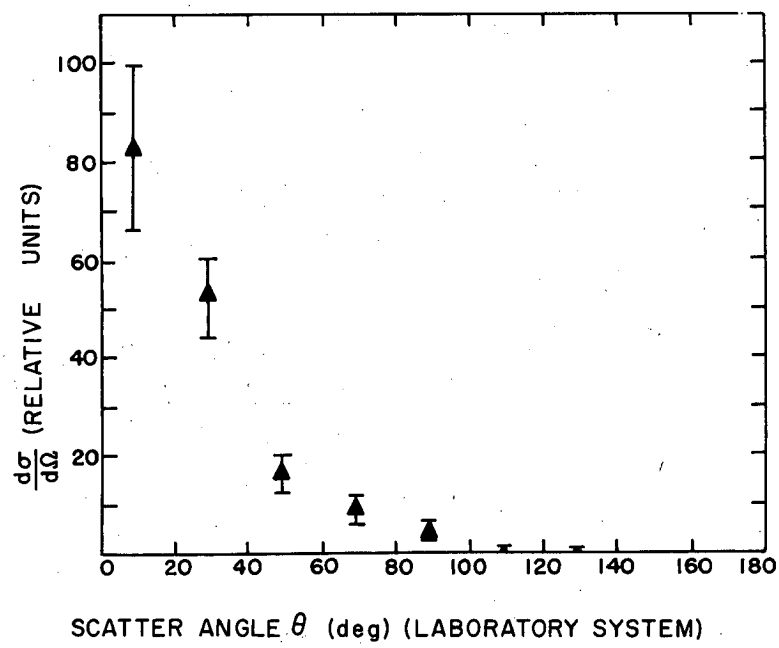

MU-14360

Fig. 3. Angular distribution of protons from $\lfloor PT \rceil$ events.

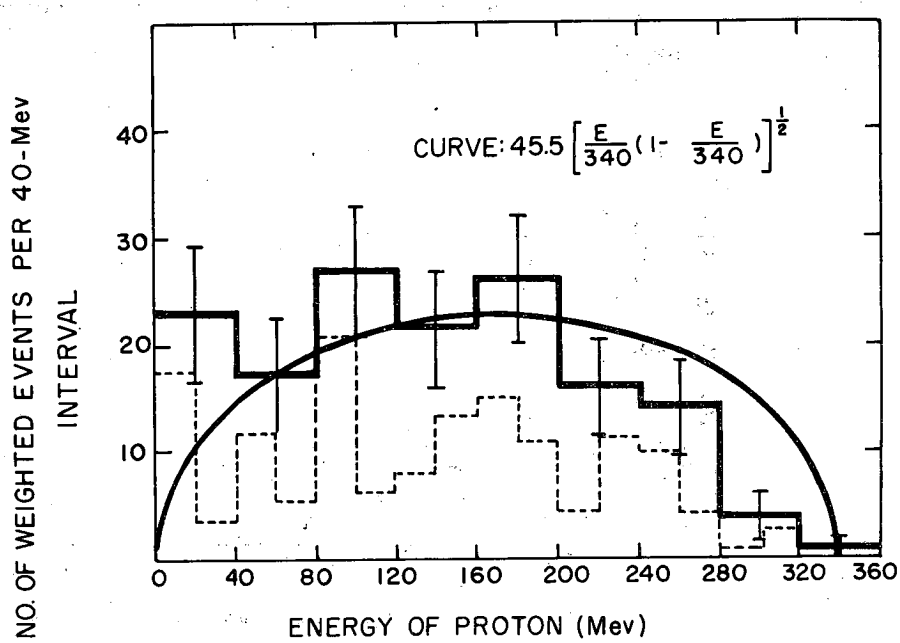

MU-14361

Fig. 4. Energy distribution of protons from [PT] events.

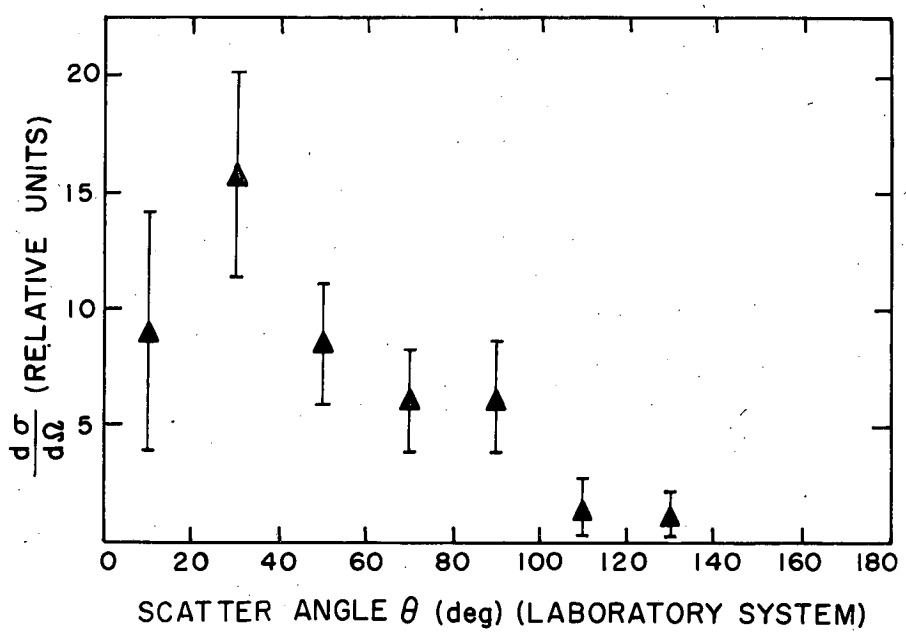

MU-14362

Fig. 5. Angular distribution of deuterons from [PD] events.

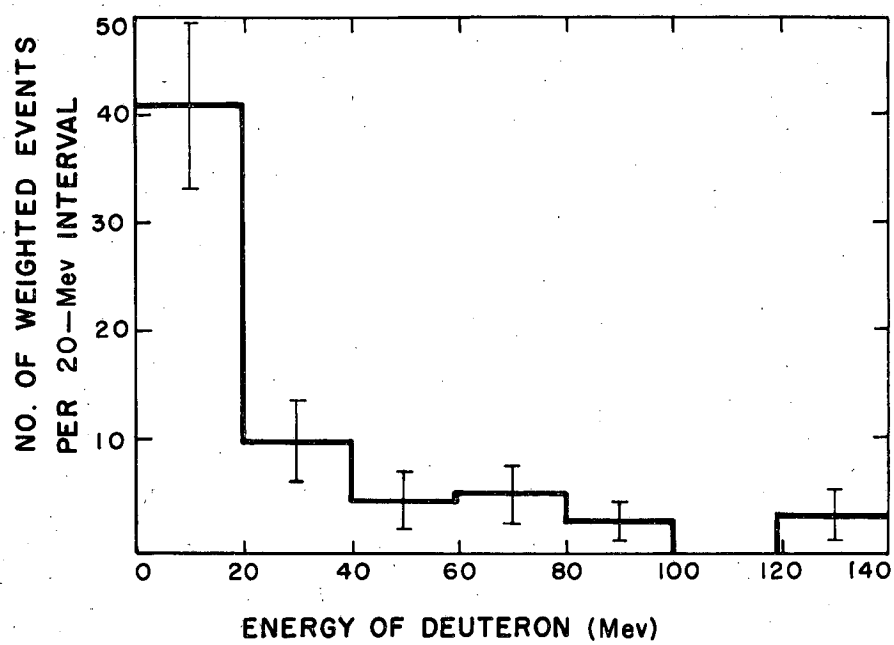

MU-14363

Fig. 6. Energy distribution of deuterons from [PD] events.

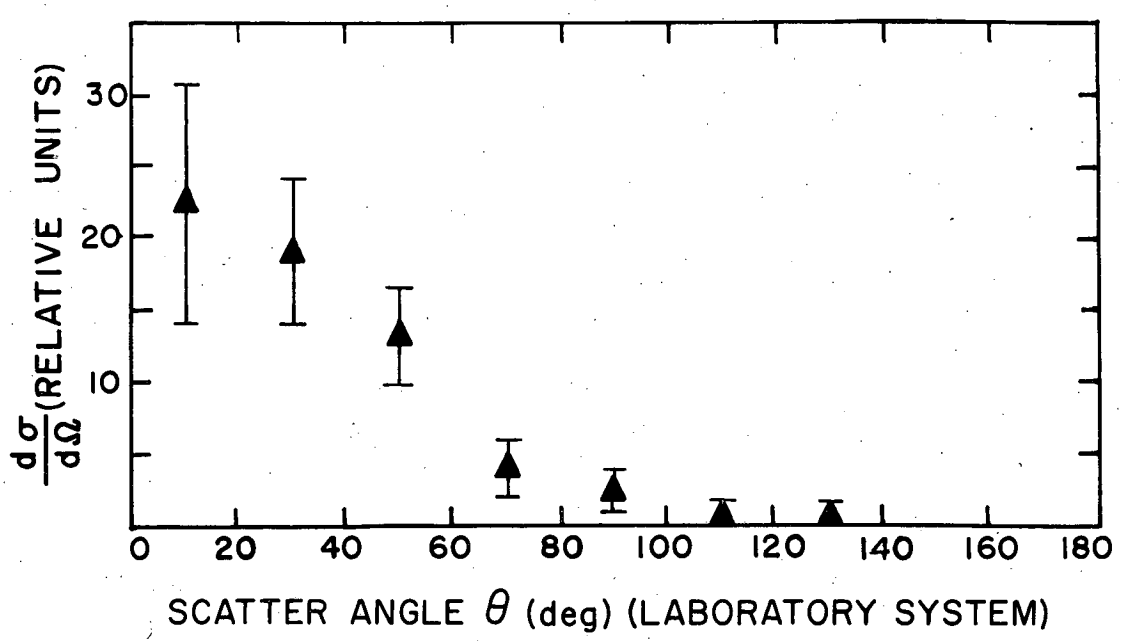

MU-14364

Fig. 7. Angular distribution of protons from [PD] events.

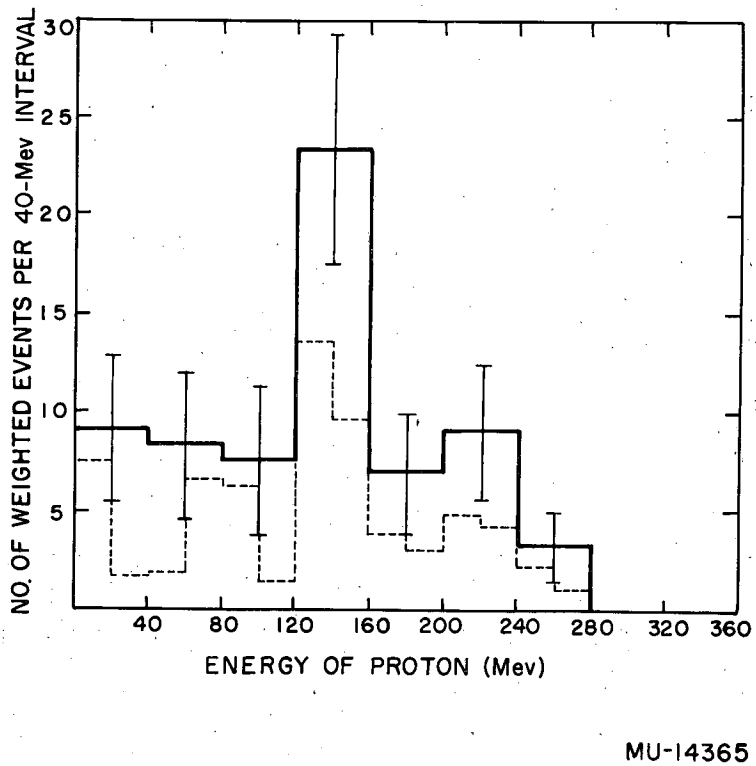

Fig. 8. Energy distribution of protons from [PD] events.

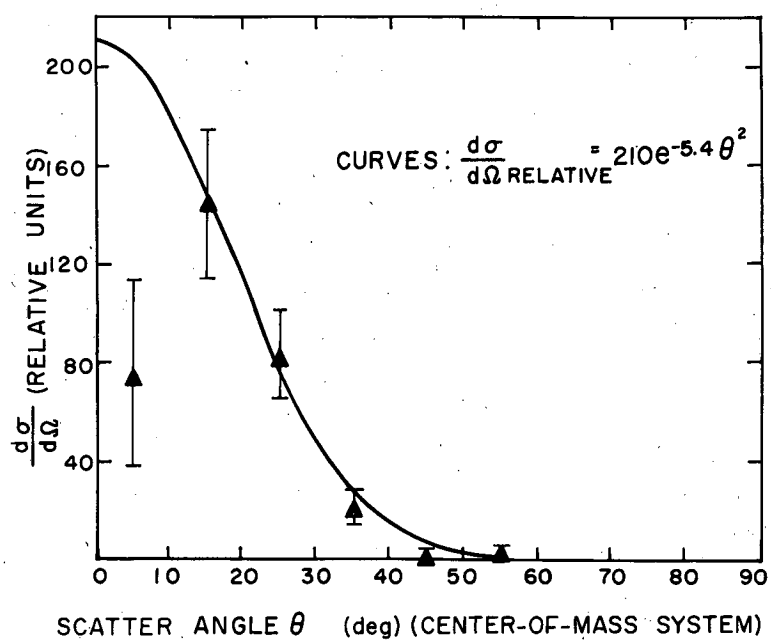

MU-14366

Fig. 9. Angular distribution of elastically scattered neutrons with energy greater than 160 Mev.

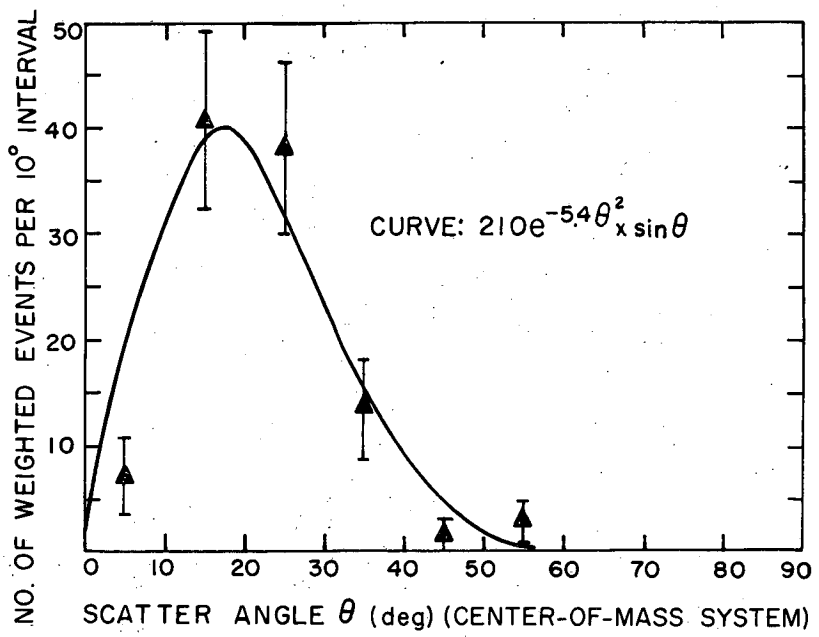

MU-14367

Fig. 10. Angular distribution of elastically scattered neutrons for incident neutrons with energy greater than 160 Mev.

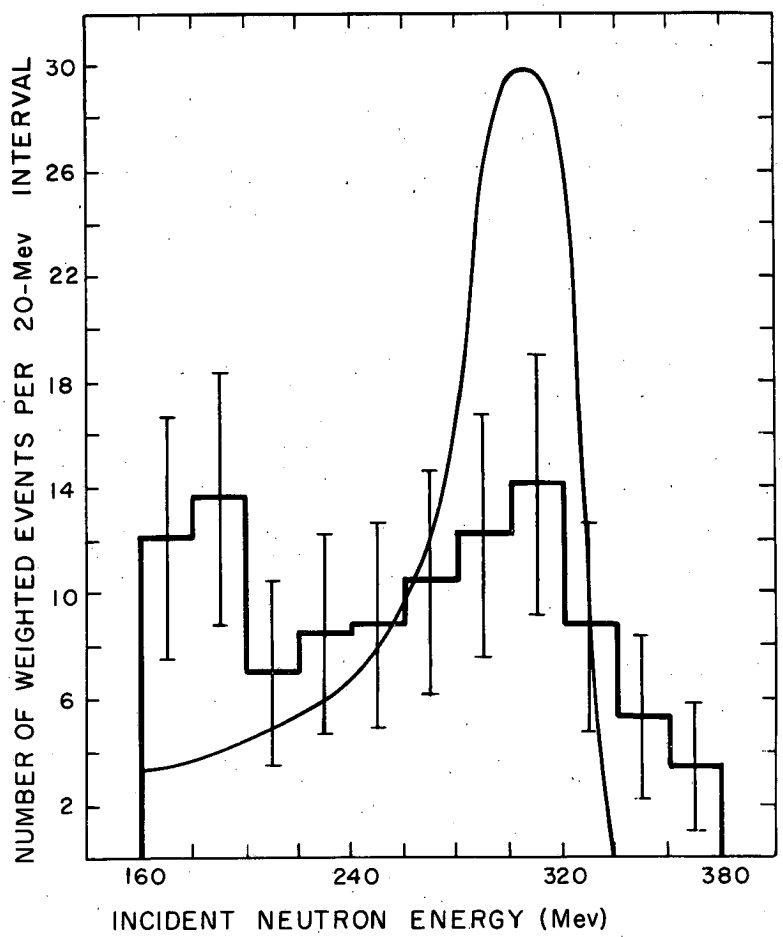

MU-14368

Fig. 11. Energy distribution of the incident neutrons, from He^4 recoils. The solid curve is De Pangher's neutron energy spectrum.

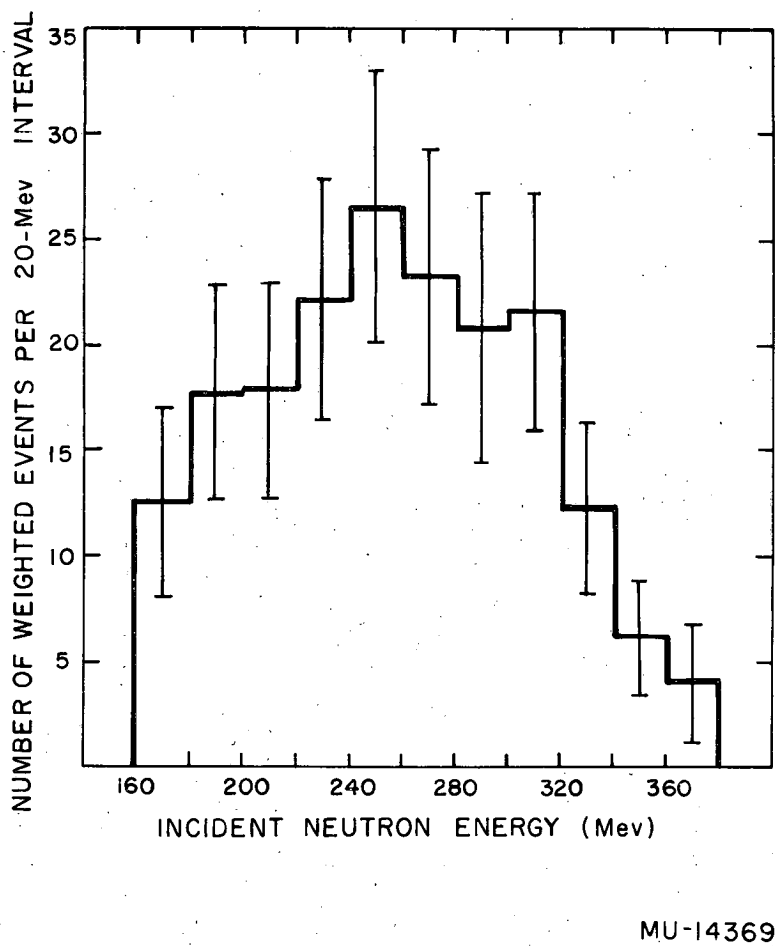

Fig. 12. Energy distribution of the incident neutrons from [PT], [DD], [DT] events.

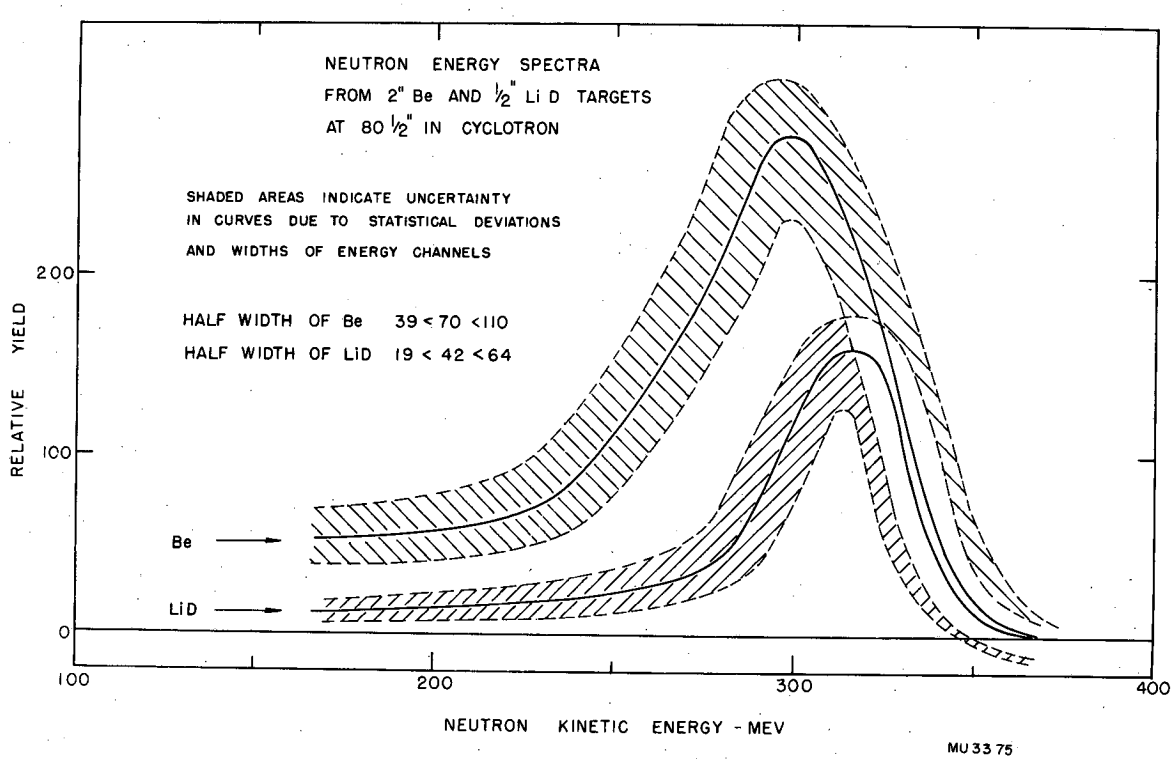

Fig. 13. Energy spectrum of neutrons from a 1/2-inch LiD target.

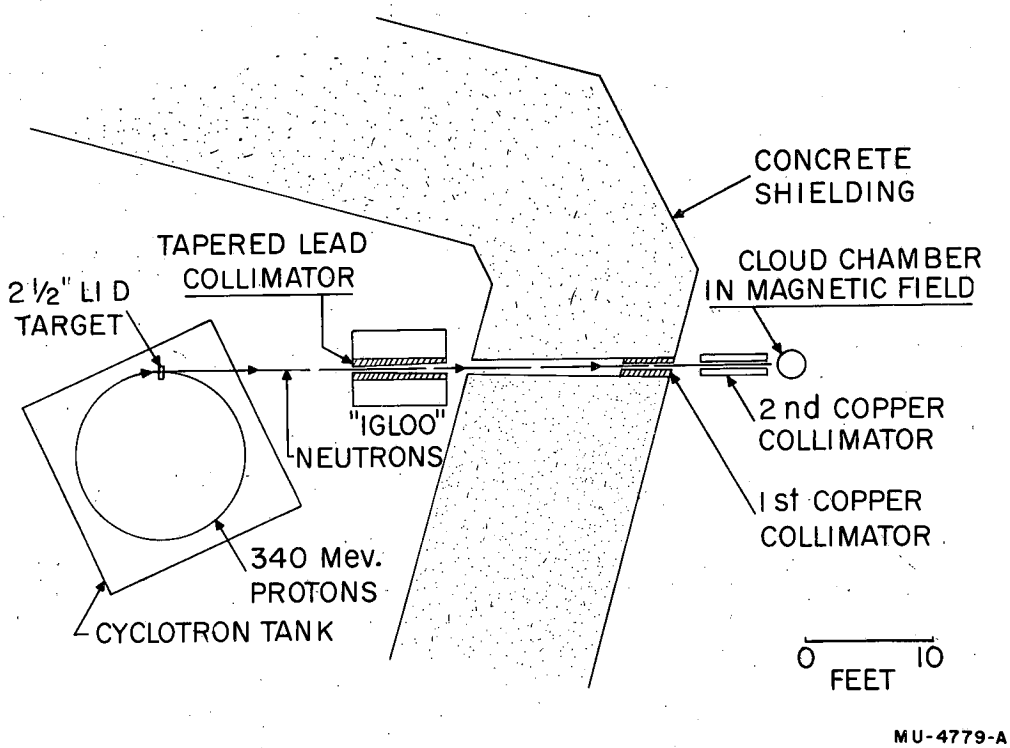

Fig. 14. Collimating system.

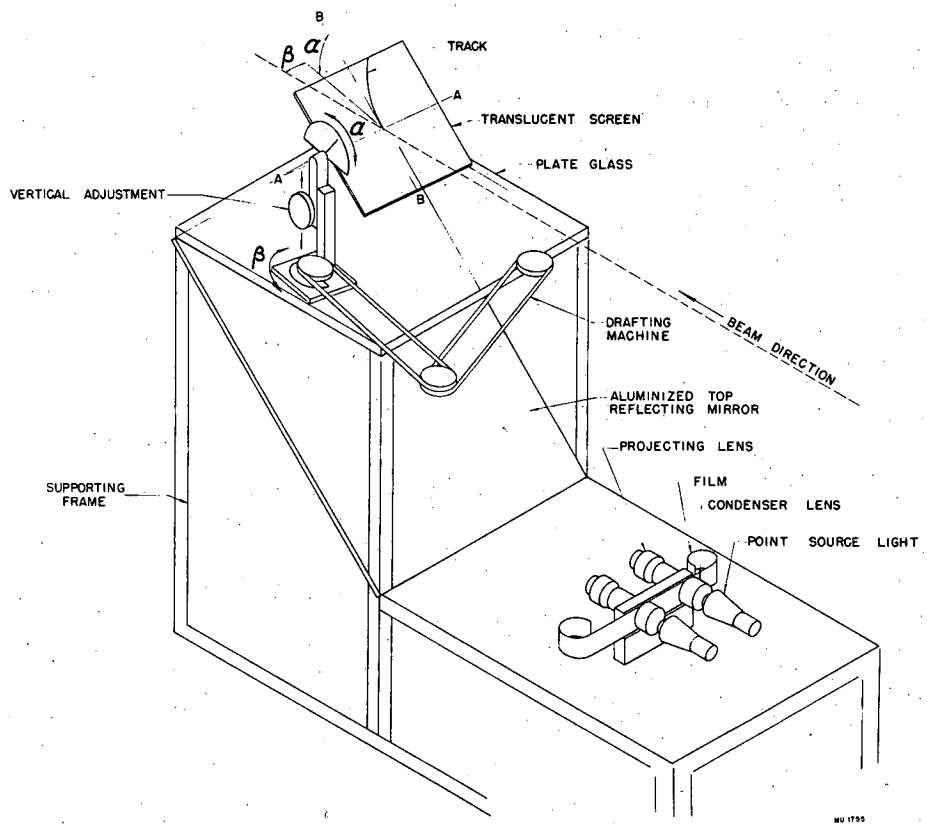

Fig. 15. Reprojection apparatus.

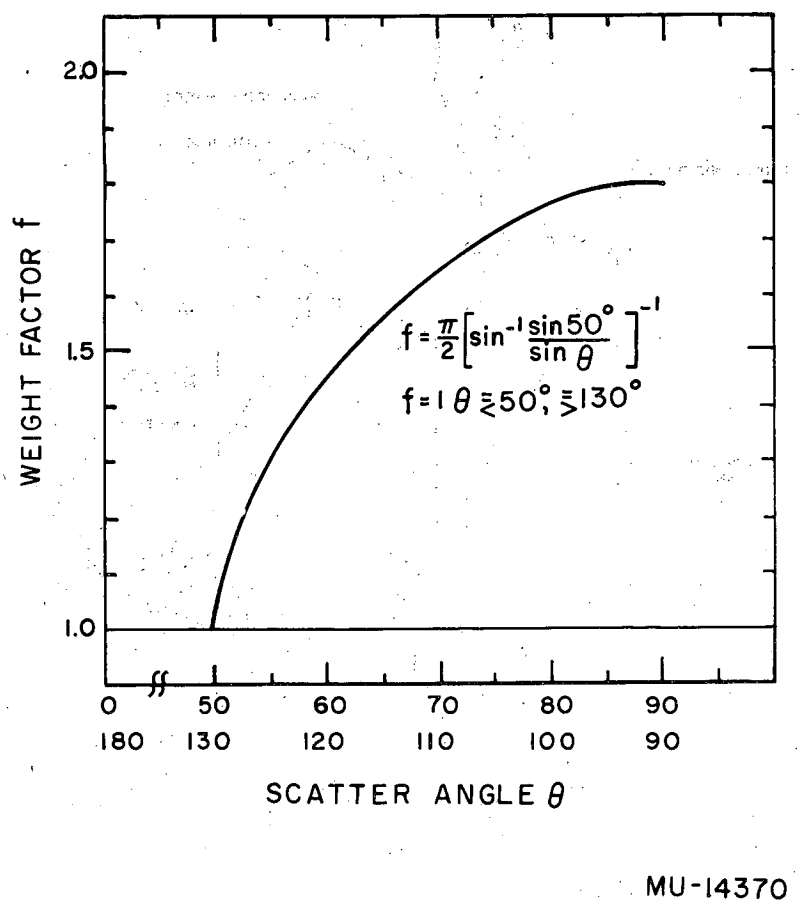

Fig. 16. Geometric correction factor for single-track events.

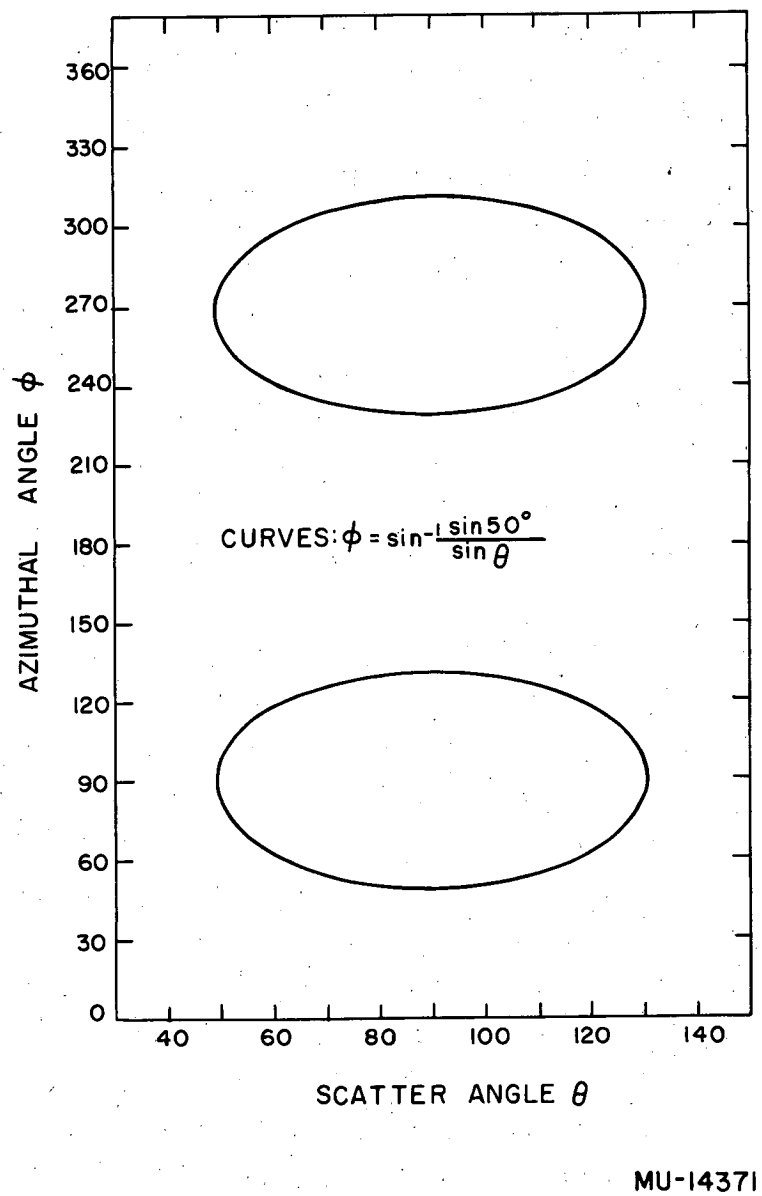

Fig. 17. Geometric correction factor diagram for two-pronged events.

REFERENCES

1. P. Tannenwald, Phys. Rev. 89, 508 (1953).
2. J. Tracy and W.M. Powell, Phys. Rev. 77, 594 (1950).
3. C. Swartz, Phys. Rev. 85, 73 (1952).
4. Hillman, Stahl, and Ramsey, Phys. Rev. 96, 115 (1954).
5. P.H. Moulthrop, Phys. Rev. 99, 1509 (1955).
6. J. Heidmann, Phil. Mag. 41, 444 (1950).
7. J. Heidmann, Compt. rend. 234, 1446 (1952).
8. W.M. Powell, Rev. Sci. Instr. 20, 403 (1949).
9. Wilson M. Powell, Scattering of High-Energy Deuterons by 90-Mev Neutron, in UCRL-1191, March 1951, p. 3.
10. Brueckner, Hartsough, Hayward, and Powell, Phys. Rev. 75, 555 (1949).
11. J.F. Tracy, Cloud Chamber Studies of the Stars in Oxygen (M.S. Thesis), Dept. of Electrical Engineering, Univ. of California), UCRL-321, April 1949.
12. N.N. Das Gupta and S.K. Ghosh, Revs. Modern Phys. 18, 225 (1946).
13. Donald Johnson, Energy and Ionization of Light Particles as a Function of Hρ, UCRL-1445, Aug. 1951.
14. John De Pangher, Jrs., A High-Pressure Cloud-Chamber Investigation of Protons Scattered by 300-Mev Neutrons (Thesis) UCRL-2153, March 1953.
15. M.S. Livingston and H.A. Bethe, Revs. Modern Phys. 9, 261 (1937).
16. W.A. Aron, B.G. Hoffman, and F.C. Williams, Range-Energy Curves, United States Atomic Energy Commission Report No. AECU-663 (UCRL-121) (2d rev.), 1949.
17. H.A. Bethe, "Range-Energy Curves: Alpha-Particles, Protons and Mesons", United States Atomic Energy Commission Report No. AECU-347, (BNL-T-7), June 1949.
18. A.E. Taylor, Phys. Rev. 92, 1071 (1953).

19. J. DeJuren, Phys. Rev. 80, 27 (1950).
20. Fox, Leith, Wouters, and MacKenzie, Phys. Rev. 80, 23 (1950).
21. V.A. Nedzel, Phys. Rev. 94, 174 (1954).
22. J. Heidmann, private communication to P. Tannenwald (see Ref. 1).
23. J. Heidmann, private communication to C. Swartz (see Ref. 3).
24. J. DeJuren and B.J. Moyer, Phys. Rev. 81, 919 (1951).
25. Ball, Moyer, and Richardson, Phys. Rev. 92, 539 (1953).
26. G.F. Chew and M.L. Goldberger, Phys. Rev. 77, 470 (1950).
27. J. Heidmann, Phys. Rev. 80, 171 (1950).
28. W.N. Hess and B.J. Moyer, Phys. Rev. 101, 337 (1956).
29. William P. Ball, Nuclear Scattering of 300-Mev Neutrons (Thesis), UCRL-1938, Aug. 1952.
30. Millburn, Birnbaum, Crandall, and Schecter, Phys. Rev. 95, 1268 (1954).
31. Fernbach, Serber, and Taylor, Phys. Rev. 75, 1352 (1949).
32. Franklin C. Ford, The Production of Charged Pi Mesons by Neutrons on Oxygen (Thesis), UCRL-2148, March 1953.
33. Myron W. Knapp, Negative Pions from Neutron Bombardment of Deuterons (Thesis), UCRL-2799, Nov. 1954.
34. J. De Pangher, Phys. Rev. 99, 1447 (1955).
35. M.O. Fuller, Phys. Rev. 98, 274 (1955).